AD-A111 174 AIR FORCE INST OF TECH WRIGHT-PATTERSON AFB OH SCHOO--ETC F/G 10/2
THEORETICAL ANALYSIS OF AN ALGAAS/ALGAAS HETEROFACE BACK-BARRIE--ETC(U)
DEC 81 D J MIAZZA
UNCLASSIFIED AFIT/GEO/PH/81D-4 NL

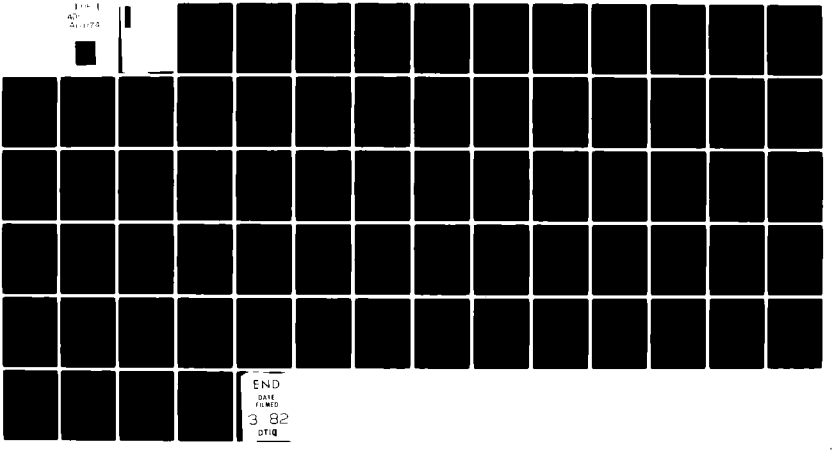

END
DATE FILMED
3 82
DTIC

AFIT/GEO/PH/81D-4

THEORETICAL ANALYSIS OF AN AlGaAs/AlGaAs HETEROFACE BACK-BARRIER SOLAR CELL

THESIS

AFIT/GEO/PH/81D-4 David J. Miazza
2nd Lt USAF

AFIT/GEO/PH/81D-4

THEORETICAL ANALYSIS OF AN AlGaAs/AlGaAs HETEROFACE BACK-BARRIER SOLAR CELL

THESIS

Presented to the Faculty of the School of Engineering
of the Air Force Institute of Technology
Air University
in Partial Fulfillment of the
Requirements for the Degree of
Master of Science

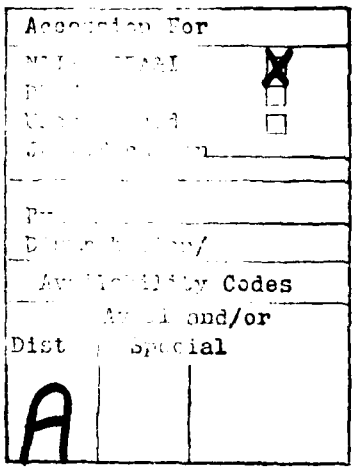

by

David J. Miazza, B.S.
2nd Lt USAF
Graduate Electro-Optics
December 1981

Approved for public release; distribution unlimited

Preface

This study arose from the Air Force's need for high efficiency solar cells for space applications. The project was proposed by Dr William P. Rahilly of the Aero Propulsion Laboratory and thanks are due him for his guidance and significant contributions.

David J. Miazza

Contents

Contents (Contd)

List of Figures

List of Tables

Abstract

A solar cell with a high band gap window, a homojunction, and a back-barrier on a base has been analyzed theoretically under fairly general conditions. The carrier transport equations were solved to obtain the short circuit current density. The theoretical results are applicable to similarly structured cells made from other materials. Although there is a lack of data on the properties of AlGaAs, many of the properties of AlGaAs have been modeled in this report by drawing on the work of others. The AlGaAs solar cell was modeled on a computer and certain design parameters (such as Al *content*) varied in order to examine their effects.

I Introduction

Recent research on AlGaAs (Aluminum Gallium Arsenide) indicates that it may be a superior material for use in solar cells (Ref 2;4) AlGaAs is similar to GaAs in structure and properties. It is anticipated that fabrication techniques already developed for GaAs cells could be adapted to AlGaAs. In this report a particular multilayer AlGaAs solar cell is analyzed theoretically, and some of its characteristics investigated by computer modeling.

Background

Single crystal GaAs is a III-V compound that forms in the zinc-blende structure. Ideally each Ga atom is surrounded by four As atoms, and each As atom is surrounded by four Ga atoms. In AlGaAs some of the Ga atoms are replaced by Al atoms. AlGaAs is also a III-V compound since Al and Ga are both Column III elements. The amount of Al is indicated by writing $Al_XGa_{1-X}As$, where X is the fraction of Ga sites of the lattice that are occupied by Al atoms.

The primary effect of replacing some of the Ga with Al is to increase the band gap energy, Eg. As X increases from 0 to 1 Eg increases from 1.424 eV to 2.168 eV (Ref 8). As will be shown later, a larger Eg in an AlGaAs solar cell leads to a larger open circuit voltage but a smaller short circuit current. The efficiency of a cell is approximately proportional to the product of the short circuit current and open circuit voltage. Calculations based on the effect of Eg on short circuit current and the current-voltage characteristic under AMO conditions (earth orbit space sunlight) at room temperature predict a maximum efficiency for cells made from materials with Eg

near 1.5 eV(Ref 1:208;3:3). An optimum value of X near .1 was expected for an $Al_XGa_{1-X}As$ solar cell, since this corresponds to a band gap, Eg, of about 1.55 eV (Ref 8). However, many other material parameters depend on X and these also affect efficiency. A major part of this report is the modeling of these parameters.

Solar Cell Structure

The structure of the solar cell analyzed and modeled in this report is shown in Figure 1a. The energy diagram is illustrated in Figure 1b. There is an anti-reflection coating on the front. Regions 1 and 2 are p-type while regions 3, 4, and 5 are n-type, so the cell is a p on n solar cell with the p-n junction at y_2. The first layer, region 1, is a window. It is thin and has a high Al content (X > .85) and, therefore, a high indirect band gap, such that it will pass almost all incident light. Its primary purpose is to effectively eliminate the loss of photogenerated minority carriers due to surface recombination at the front surface. Even when chemically treated (application of an anti-reflective coating) there may remain a large concentration of surface states on the front of the cell. However, the high band gap window acts as a barrier to keep photogenerated electrons in region 2 from reaching the front surface and recombining with holes. The window constrains the electrons to region 2 and increases the probability of their reaching the p-n junction at y_2. The width of region 1 is selected to be .3μ, large enough so that tunneling of electrons from region 2 to the front surface can be neglected, but not too large because it is preferable to pass most of the incident light to regions that are closer to the junction. High band gap AlGaAs windows are already being used on GaAs cells (Ref 15).

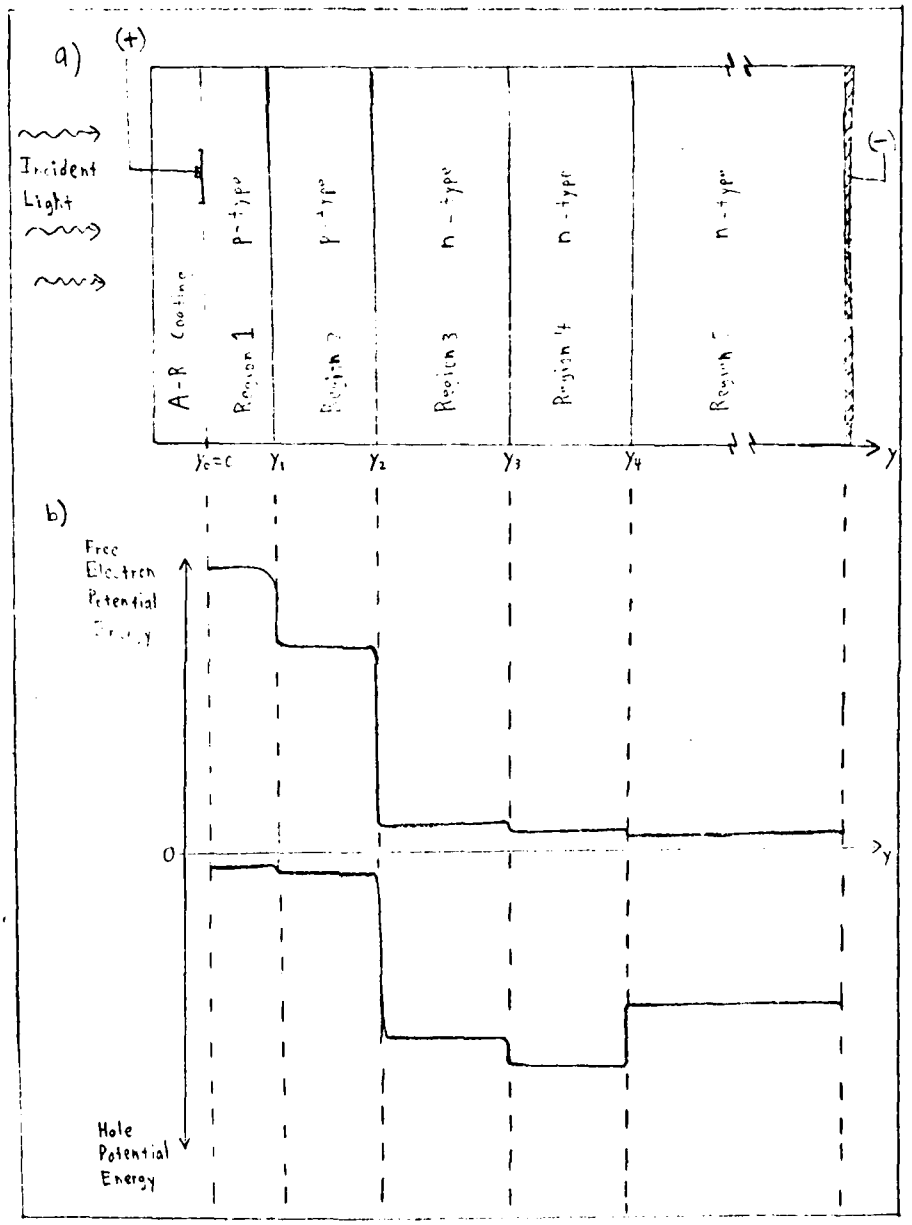

Figure 1. a) Structure of AlGaAs Solar Cell
b) Energy Diagram of AlGaAs Solar Cell

Regions 2 and 3 are lower band gap layers (X < .3). Both layers have the same Al content so that the junction between them is a homojunction. Most of the absorption of light and resultant photogeneration of electron-hole pairs takes place in these two regions. The Al content, X, is chosen to be less than .3. This simplifies analysis because at higher Al content (.35 < X < .6) the direct and indirect bands are close together (Ref 4:CS-5). The maximum efficiency was expected for X near .1 as mentioned previously. Region 4 has X = .3 so that its band gap is larger than that of region 3. It will constrain holes in region 3 to move toward the junction. Region 5 is the GaAs base upon which the other layers are grown and is used because of lattice matching and its availability in single crystal form. Region 5 has a lower band gap than region 4. It will be shown that region 4 causes region 5 to be isolated from the other regions, so that it has no affect on the characteristics of the solar cell.

Organization of Report

The second chapter of this report is a fairly general derivation of the short circuit current density in terms of a few parameters for a solar cell which has an energy diagram like that of Figure 1b. Few assumptions are made and the results are applicable to similarly structured cells made from other materials. In Chapter 3 the diode current is introduced, and the total current as a function of voltage and the efficiency are examined. The treatment is still fairly general.

In Chapter 4 the parameters affecting the current and efficiency of the solar cell are modeled. Certain design parameters are specified while others are left as variables. The model of the solar cell is then much more specific. In Chapter 5 a brief description is given of

the program or computer model of the AlGaAs solar cell. The program is merely the compilation of the results of Chapters 2, 3, and 4. It generates some of the characteristics, such as efficiency, of the AlGaAs solar. Its input variables are the design parameters which have not yet been specified, such as the width of various regions and the Al content of region 2 and 3. Chapter 5 also gives the results of varying some of these parameters, and these results are examined.

In Chapter 6 the overall conclusions and recommendations are made.

II Short Circuit Current Density

The short circuit or photogenerated current density, $J^T_{s,c.}$, is due to the diffusion of charge carriers, holes and electrons. The carrier transport equations, which govern the net flow of electrons and holes in semiconductors, will be derived in the first section of this chapter. In the second section these equations will be applied to a solar cell with the energy diagram given in Figure 1b. The equations will be solved for $J^T_{s.c.,}$. In the third section the results will be analyzed.

Carrier Transport Equation

In a non-magnetic media two of Maxwell's equations may be written as

$$\nabla \cdot D = \rho \tag{1}$$

$$\nabla \times H = J + \frac{\partial D}{\partial t} \tag{2}$$

where

D = electric displacement vector

H = magnetic intensity vector

J = current density vector

ρ = free charge density

Taking the divergence of the Eqn (2) gives

$$0 = \nabla \cdot J + \frac{\partial}{\partial t} \nabla \cdot D \tag{3}$$

since the divergence of the curl of any vector is zero. Substituting Eqn (1) into Eqn (3) yields

$$\nabla \cdot J = - \frac{\partial \rho}{\partial t} \tag{4}$$

This is the continuity equation for free charges. The volume integral of $\nabla \cdot J$ is the rate of charge leaving the volume, while the volume integral of $-\frac{\partial \rho}{\partial t}$ represents the rate of decrease of charge in the volume.

There are two kinds of free carriers in the semiconductor. Electrons move about in the conduction band and holes are transported in the valence band. Thus

$$\rho = q\,(P-N) \tag{5}$$

where

q = the elementary charge (1.6×10^{-19} coulombs)

P = density of holes ($\#/cm^3$)

N = density of electrons ($\#/cm^3$)

The current density, J, can be broken up into terms for the drift and diffusion of holes and electrons

$$J = J^p_{drift} + J^p_{diff} + J^N_{drift} + J^N_{diff} \tag{6}$$

The drift current densities come from Ohm's Law and are due to the net drifting of charge carriers in an electric field E.

$$J^p_{drift} = q\mu_p EP \tag{7}$$

$$J^N_{drift} = q\mu_n EN \tag{8}$$

where

μ_p = mobility of holes (cm^2/volt-sec)

μ_n = mobility of electrons (cm^2/volt-sec)

The diffusion current densities are based on Fick's Law and are due to the average flow from a region of high concentration to region of

low concentration. In symbolic form

$$J^P_{diff} = - qD_p \nabla P \tag{9}$$

$$J^N_{diff} = qD_n \nabla N \tag{10}$$

where

D_p = diffusivity of holes (cm^2/sec)

D_n = diffusivity of electrons (cm^2/sec)

Eqn (4) may now be rewritten using Egns (5) through (10) as

$$\nabla \cdot (\mu_p EP - D_p \nabla P + \mu_n EN + D_n \nabla N) = \frac{\partial N}{\partial t} - \frac{\partial P}{\partial t} \tag{11}$$

where q has been divided out. In order to obtain separate equations governing the transport of electrons and holes from Eqn (11) carrier generation and recombination terms must be included. This is because in general the generation and recombination rate of holes and electrons are a function of both P and N. The Shockley-Hall carrier generation-recombination rate is given by

$$U = \frac{PN - n_i^2}{(P+P_t)\tau_{no} + (N+N_t)\tau_{po}} \tag{12}$$

where

n_i = intrinsic carrier density (cm^{-3})

P_t, N_t = trap densities (cm^{-3})

τ_{no}, τ_{po} = carrier lifetimes (sec)

as defined by Sze (Ref 12:48). Note that since holes and electrons are oppositely charged and since both generation and recombination involve electron-hole pairs, neither generation nor recombination affect the total free charge density, ρ. Since the carriers move independently in their respective gands, Eqn (11) may be rewritten as

$$\left[\frac{\partial p}{\partial t} + \nabla\cdot(\mu_p EP - D_p \nabla P) - G + U\right]$$

$$+ \left[-\frac{\partial N}{\partial t} + \nabla\cdot(\mu_n EN + D_n \nabla N) + G - U\right] = 0 \qquad (13)$$

and each straight bracketed term can be set equal to zero. In the present application the generation rate, G, is taken to be a function of position only. Thus Eqn (13) fragments into

$$\frac{\partial P}{\partial t} + \nabla\cdot(\mu_p EP - D_p \nabla P) - G + U = 0 \qquad (14)$$

$$\frac{\partial N}{\partial t} + \nabla\cdot(-\mu_n EN - D_n \nabla N) - G + U = 0 \qquad (15)$$

Eqns (14) and (15) are the carrier transport equations for holes and electrons respectively. They are coupled by the recombination rate, U, given in Eqn (12) and the electric field vector E. Using the relation $D = \varepsilon E$, where ε = permittivity, in Eqn (1) gives the third equation needed to determine E, P, and N. However, the electric field will be assumed to be zero so that only Eqns (14) and (15) are needed.

Solution of the Transport Equations

If the solar cell is unilluminated it is merely a diode. In a given region and with no external voltage bias, the electron and hole concentrations will be at their thermal equilibrium values N_o and P_o respectively. The short circuit current density will be zero. If the cell is illuminated the concentrations are increased to $N = N_o + n$ and $P = P_o + p$, where n and p are the excess electron and hole concentrations due to photogeneration. The short circuit current or light generated current is due to the excess carriers. In order to obtain $J^T_{s.c.}$ the excess minority carrier concentrations in each region must be found.

In Figure 1b the energy band edges for the electrons and holes change near the edges of each region but are constant in between. The energy bands will be assumed to change abruptly at each interface, except in Chapter 3 where the carrier depletion width at the p-n junction will be used to obtain the diode current. Actually the energy bands change over a small width and an electric field (proportional to the gradient of the energy band edge) exists there. Since the energy bands are constant with position in each region no electric field exists. Therefore, in a given region assuming time independence Eqn (15) can be written as

$$D_n \nabla^2 N + G - U = 0 \tag{16}$$

Photogeneration is the interaction of a photon and an electron in the valence band which raises the electron to the conduction band and leaves a hole in the valence band. It is assumed that no other absorption processes (such as free carrier absorption) are insignificant for the wavelengths of interest (.35μ to .90μ). At a particular wavelength of light the generation rate G is proportional to the flux of photons at that wavelength. However, the photon flux decreases with increasing y due to absorption.

At present only one wavelength of light, λ, will be considered. Let F_1 be the flux of photons at λ incident on the very front of region 1. The photon flux in region 1 can be written as $F_1 e^{-\alpha_1 y}$, where α_1 is the absorption coefficient at λ. Since the generation rate of carriers is equal to the absorption rate of photons, from Beer's Law

$$G_1 = \alpha_1 F_1 e^{-\alpha_1 y} \tag{17}$$

The y dimension of each layer of the solar cell is much smaller than its other two dimensions, and since the generation rate varies only with y, the carrier densities will be assumed to vary only with y. In addition, since N_o is constant in a given region the variation of N with y is due solely to n the excess electron concentration. In region 1 Eqn (16) can now be written as

$$D_{n1} \frac{\partial^2 n_1}{\partial y^2} - U_1 = - \alpha_1 F_1 e^{-\alpha_1 y} \tag{17}$$

In a p-type region $P_o >> N_o$. The excess carriers due to photo-generation have little effect on P compared to the effect on N.

$$P = P_o + p \approx P_o \tag{18}$$

$$N = N_o + n \tag{19}$$

Since the term $P\tau_{no}$ dominates in the denominator of Eqn (12) and since $n_1^2 = P_o N_o$, the recombination rate in region 1 reduces to

$$U_1 \approx \frac{n_1}{\tau_{n_{o1}}} \tag{20}$$

Substituting into Eqn (17) yields

$$D_{n1} \frac{\partial^2 n_1}{\partial y^2} - \frac{n_1}{\tau_{n_{o1}}} = - \alpha_1 F_1 e^{-\alpha_1 y} \tag{21}$$

The diffusion length of a carrier is related to the diffusivity and lifetime by

$$L = D\tau \tag{22}$$

Therefore Eqn (21) can be written as

$$D_{n1} \frac{\partial^2 n_1}{\partial y^2} - \frac{D_{n1} n_1}{L_{n_1}^2} = -\alpha_1 F_1 e^{-\alpha_1 y} \tag{23}$$

Equations similar to this may be written for regions 2, 3, and 4.

$$D_{n2} \frac{\partial n_2}{\partial y^2} - \frac{D_{n2} n_2}{L^2_{n_2}} = - \alpha_2 F_2 e^{-\alpha 2(y-y_1)} \tag{24}$$

$$D_{p3} \frac{\partial p_3}{\partial y^2} - \frac{D_{p3} p_3}{L^2_{p_3}} = - \alpha_3 F_3 e^{-\alpha 3(y-y_2)} \tag{25}$$

$$D_{p4} \frac{\partial p_4}{\partial y^2} - \frac{D_{p4} p_4}{L^2_{p_4}} = - \alpha_4 F_4 e^{-\alpha 4(y-y_3)} \tag{26}$$

where $F_k = F_{k-1}\, e^{-\alpha k-1(y_{k-1}-y_{k-2})}$ is the photon flux incident on the front of region k. Eqns (23) through (24) along with boundary conditions not yet introduced determine the excess minority carrier concentrations in regions 1 through 4. The term on the right hand side of each equation is the forcing term. It determines the particular solution to the differential equation.

Since it is the minority carriers in each region that are of primary interest, the subscripts p and n will be dropped when only minority carriers are being discussed.

The solutions to Eqns (23) through (26) are

$$n_1(y) = A_1 \cosh \left(\frac{y-y1}{L_1}\right) + B_1 \sinh \left(\frac{y-y1}{L_1}\right) + C_1 e^{-\alpha_1 y} \tag{27}$$

$$n_2(y) = A_2 \cosh \left(\frac{y-y2}{L_2}\right) + B_2 \sinh \left(\frac{y-y2}{L_2}\right) + C_2 e^{-\alpha 2(y-y1)} \tag{28}$$

$$p_3(y) = A_3 \cosh \left(\frac{y-y2}{L_3}\right) + B_3 \sinh \left(\frac{y-y2}{L_3}\right) + C_3 e^{-\alpha 3(y-y2)} \tag{29}$$

$$p_4(y) = A_4 \cosh \left(\frac{y-y3}{L_4}\right) + B_4 \sinh \left(\frac{y-y3}{L_4}\right) + C_4 e^{-\alpha 4(y-y3)} \tag{30}$$

where

$$C_k = \frac{\alpha_k F_k}{D_k(\frac{1}{L_k^2} - \alpha_k^2)} \tag{31a}$$

$$F_k = F_{k-1} e^{-\alpha_{k-1} Z_{k-1}} \quad \text{for } k = 2,3,4 \tag{31b}$$

In each of Eqns (27) through (30) the first two terms are together the homogeneous solution. The coefficients A_k and B_k are as yet unspecified. They will be determined from the appropriate boundary conditions for each region. The homogeneous solutions could have been written in other forms since the coefficients are not yet specified; however, the form used here makes application of the boundary conditions simpler. The third term in each equation is the particular solution. Eqns (27) through (30) can be verified by substituting them into Eqns (23) through (26).

There are eight B.C.s (boundary conditions) in the solar cell which determine the eight coefficients A_k and B_k ($k = 1,2,3,4$). At the front of region 1 electron-hole pairs can recombine via surface recombination states. Since time independence is assumed the rate of excess electrons recombining at the surface must equal the rate at which electrons are diffusing to the surface.

$$D_1 \frac{dn_1(o)}{dy} = S_o \, n_1(o) \tag{32}$$

where S_o is the surface recombination velocity of electrons at $y = 0$.

At y_1 there is an electric field which rapidly transfers electrons across the interface from region 1 to region 2. It acts as a drain and drives the excess electron concentration to zero on the left side of the interface. The B.C. at y_1^- is

$$n_1(y_1) = 0 \tag{33}$$

The rate of excess electrons coming out of the surface on the right side must equal the rate going in on the left side minus the rate at which they are lost due to interface recombination states. Therefore

$$D_2 \frac{dn_2(y_1)}{dy} = D_1 \frac{dn_1(y_1)}{dy} + S_1 n_2(y_1) \tag{34}$$

At y_2, the junction, another electric field exists which ties the excess electron concentration to zero on the left side.

$$n_2(y_2) = 0 \tag{35}$$

Using similar arguments similar B.C.s result for the excess hole density on the p side of the solar cell;

$$p_3(y_2) = 0 \tag{36}$$

$$D_4 \frac{dp_4(y_3)}{dy} = D_3 \frac{dp_3(y_3)}{dy} + S_3 p_3(y_3) \tag{37}$$

$$p_4(y_3) = 0 \tag{38}$$

$$p_4(y_4) = 0 \tag{39}$$

The integration constants for $P_4(y)$ are determined by Eqns (38) and (39). The hole density in region 4 is affected by the other regions only through F_4 which is affected by the absorption of light in the preceding regions. $p_4(y)$ affects $p_3(y)$ through Eqn (37). Similarly $n_1(y)$ is independent of the other regions but it affects $n_2(y)$ through Eqn (34).

The following definitions are made for convenience:

$$z_k = y_k - y_{k-1} = \text{width of region k} \tag{40}$$

$$U_1 = \cosh\left(-\frac{z_1}{L_1}\right), \quad V_1 = \sinh\left(-\frac{z_1}{L_1}\right) \tag{41-42}$$

$$U_2 = \cosh\left(-\frac{z_2}{L_2}\right), \quad V_2 = \sinh\left(-\frac{z_2}{L_2}\right) \tag{43-44}$$

$$U_3 = \cosh\left(\frac{z_3}{L_3}\right) \quad , \quad V_3 = \sinh\left(\frac{z_3}{L_3}\right) \tag{45-46}$$

$$U_4 = \cosh\left(\frac{z_4}{L_4}\right) \quad , \quad V_4 = \sinh\left(\frac{z_4}{L_4}\right) \tag{47-48}$$

U here should not be confused with the recombination rate given in Eqn (12).

The direction of positive current will be taken as the negative y direction. The following current densities are pertinent:

$$J_1 = -q\, D_1 \frac{dn_1(y_1)}{dy} = -q\, D_1 \left(\frac{B_1}{L_1} - \alpha_1 C_1 e^{-\alpha_1 z_1}\right) \tag{49}$$

$$J_2 = -q\, D_2 \frac{dn_2(y_2)}{dy} = -q\, D_2 \left(\frac{B_2}{L_2} - \alpha_2 C_2 e^{-\alpha_2 z_2}\right) \tag{50}$$

$$J_3 = q\, D_3 \frac{dp_3(y_2)}{dy} = q\, D_3 \left(\frac{B_3}{L_3} - \alpha_3 C_3\right) \tag{51}$$

$$J_4 = q\, D_4 \frac{dp_4(y_3)}{dy} = q\, D_4 \left(\frac{B_4}{L_4} - \alpha_4 C_4\right) \tag{52}$$

J_1 is the electron current density at y_1^-. It represents the injection of electrons from region 1 into region 2. J_2 is the electron current density at y_2^-. It represents the electrons flowing into the junction from region 2. J_3 is the hole current density at y_2^+. It represents the holes flowing into the junction. Finally, J_4 is hole current density at y_3^+. It represents the injection of holes from region 4 into region 3.

The A_k and B_k coefficients can now be presented in a way that is actually much less painful than might otherwise be possible. The result of applying the B.C.s, Eqns (32) through (34) and the above definitions is:

$$A_1 = - C_1 e^{-\alpha_1 z_1} \tag{53}$$

$$B_1 = \frac{C_1(S_0+D_1\alpha_1 + (\frac{D_1V_1}{L_1} - S_0U_1)e^{-\alpha_1 Z_1})}{(\frac{D_1U_1}{L_1} - S_0V_1)} \tag{54}$$

$$A_2 = -C_2\, e^{-\alpha_2 Z_2} \tag{55}$$

$$B_2 = \frac{-\frac{J_1}{q} + C_2\,(S_1 + D_2\alpha_2 + (\frac{D_2V_2}{L_2} - S_1U_2)e^{-\alpha_2 Z_2})}{\frac{D_2U_2}{L_2} - S_1V_2} \tag{56}$$

$$A_3 = -C_3 \tag{57}$$

$$B_3 = \frac{\frac{J_4}{q} + C_3\,((-S_3 + D_3\,\alpha_3)e^{-\alpha_3 Z_3} + \frac{D_3V_3}{L_3} + S_3U_3)}{\frac{D_3U_3}{L_3} + S_3V_3} \tag{58}$$

$$A_4 = -\,C_4 \tag{59}$$

$$B_4 = C_4\,(\frac{U_4 - e^{\alpha_4 Z_4}}{V_4}) \tag{60}$$

These are the coefficients that were needed in Eqns (27) through (30). The excess minority carrier concentrations in regions 1 through 4 have now been determined. However, it is the current densities that are of primary interest. Using Eqns (49) through (60) the current densities may be written more explicitly as

$$J_1 = -\,q\,D_1C_1\left[\frac{S_0+D_1\alpha_1 + (\frac{D_1V_1}{L_1} - S_0U_1)e^{-\alpha_1 Z_1}}{D_1U_1 - S_0V_1L_1} - \alpha_1 e^{-\alpha_1 Z_1}\right] \tag{61}$$

$$J_2 = -\,qD_2\left[\frac{-\frac{J_1}{q} + C_2\,(S_1 + D_2\alpha_2 + (\frac{D_2V_2}{L_2} - S_1U_2)e^{-\alpha_2 Z_2})}{D_2U_2 - S_1V_2L_2} - \alpha_2 C_2 e^{-\alpha_2 Z_2}\right] \tag{61}$$

$$J_3 = qD_3 \quad \frac{\frac{J_4}{q} + C_3\left((-S_3 + D_3\alpha_3)e^{-\alpha_3 z_3} + \frac{D_3V_3}{L_3} + S_3U_3\right)}{D_3U_3 + S_3V_3L_3} - \alpha_3 C_3 \quad (63)$$

$$J_4 = q\, D_4C_4\left(\frac{U_4 - e^{-\alpha_4 z_4}}{V_4L_4} - \alpha_4\right) \quad (64)$$

The preceding derivation was done for only one wavelength of light, λ. Since the absorption coefficients are a function of λ, the spectral photon fluxes are needed. If $F_k = F_k(\lambda)$ is the spectral photon flux incident on the front of region k then the preceding derivation gives the spectral excess minority carrier densities, $n_k(\lambda)$ and $p_k(\lambda)$, and the spectral current densities $J_k(\lambda)$. The total excess minority carrier concentrations and current densities can be obtained by integrating over wavelength.

$$n_k^T = \int n_k(\lambda)\, d\lambda \quad (65)$$

$$J_k^T = \int J_k(\lambda)\, d\lambda \quad (66)$$

J_2^T is the electron current density at the p-n junction. J_3^T is the hole current density at the p-n junction. The total current density in the junction is their sum. Since time independence was assumed the carrier concentrations must remain constant with time. Therefore the total current density is the same everywhere in the cell; it does not vary with y. The short circuit or light generated current is

$$J_{s.c.}^T = J_2^T + J_3^T \quad (67)$$

Analysis of Theoretical Results

The spectral current densities J_k given in Eqns (61) through (64) are of similar form. The term $\frac{J_1 D_2}{D_2 U_2 - S_1 V_2 L_2}$ in Eqn (62) is the contribution to J_2 due to the current injection from region 1 into region 2. This contribution is less than the injection current density, J_1, since $U_2 > 1$ and $V_2 < 0$ while D_2, S_1, and L_2 are positive. The same is true for the contribution of J_4 to J_3. This is because some of the injected carriers are lost through recombination either at an interface or in the bulk of the region. The bulk recombination is represented by the diffusion lengths L_k.

Except for the contribution due to current injection, J_2 has exactly the same form as J_1. J_2 and J_3 are very similar. The difference in the form of Eqns (62) and (63) are due to the direction of light, toward the junction in region 2 and away from the junction in region 3.

As previously mentioned, the excess hole density in region 4 is independent of region 5. Since it is the slope of the excess hole density at y_3 that determines J_4^T, J_4^T is independent of region 5. Therefore J_3^T and $J_{s.c.}^T$ are also independent of region 5. This is due to the B.C. at y_4, Eqn (39), which is a result of holes in region 4 having a higher potential energy than holes in region 5. The primary purpose of region 4 is to act as a barrier, preventing holes in region 3 from moving beyond y_3 and therefore constraining them to move toward the p-n junction. However, region 4 has other effects. Another beneficial effect is the injection of holes from region 4 into region 3. The injection current density, J_4^T, will probably be small for a practical solar cell because much of the light will be absorbed before it reaches region 4. Still, several steps can be taken to optimize the current injection. J_4 can

be increased by decreasing the Al content in region 4, which increases the absorption. However, the band gap in region 4 must be greater than the band gap in region 3 in order for region 4 to act as a barrier to the holes in region 3. The band gap increases with Al content. The Al content in region 4 must be somewhat higher than the Al content in region 3 in order for the B.C.s at y_3, Eqns (37) and (38), to hold, and in order for region 4 to act as a barrier.

As mentioned in Chapter 1, it was anticipated that the greatest efficiencies would be achieved for an Al content in regions 2 and 3 of $X_{2,3}$ near .1. The Al content in region 4 was chosen to be $X_4 = .3$. Therefore, the B.C.s at y_3, Eqns (37) and (38), will be good approximations for $X_{2,3}$ up to about .25. A higher X_4 would produce a lower J_4. Also, as indicated in Chapter 1, the direct and indirect bands are close together for $.35 < x < .6$ so that modeling of some material parameters becomes very difficult at those Al contents since significant electron transport occurs in three conduction bands.

J_4 can also be optimized by adjusting the width of region 4, z_4. This could be done by varying z_4 in the computer model. A large z_4 is probably desirable, since the electric field at y_4 acts as a drain on excess holes in region 4. This drain would then be far removed from the front of the region where the photon flux is higher and where most of the photogeneration in the region takes place.

Region 4 also has an adverse affect. This is due to the recombination at y_3, which acts as a drain on the excess holes in region 3. In the worst case, when $S_3 \to \infty$, Eqn (63) reduces to

$$J_3 = q\, D_3 C_3 \left(\frac{U_3 - e^{-\alpha_3 z_3}}{V_3 L_3} - \alpha_3 \right) \qquad (68)$$

If region 4 were not included in the solar cell then regions 3 and 5 would be adjacent to each other. Region 3 has a higher Al content, larger band gap, and higher hole potential energy than region 5. Therefore the electric field at their interface would be in the positive y direction. One of the boundary conditions there would be

$$p_3(y_3) = 0 \tag{69}$$

Thus the excess hole density in region 3 would be tied to zero at both edges. This was the case for $p_4(y)$ before. J_3 would then have the same form that J_4 had in Eqn (64). But J_3 in Eqn (68) is also of that same form. J_3 is the same for both cases, changing the B.C. at y_3 to Eqn (69) or letting S_3 become infinite. Therefore, J_3 and $J_{s.c.}$ will be at least as large with region 4 included in the solar cell as without it.

III Diode Current Density and Efficiency

In this chapter the diode current density, J_D, is introduced. The total current density, J^T, and the efficiency of the solar cell are also discussed.

The depletion width, W, of the junction was neglected in determining $J^T_{s.c.}$. W is very small and little photogeneration takes place in the junction. However, W is important in determining J_D. If dopants with low diffusion coefficients are used, and the doping levels on both sides of the junction are high, the junction can be assumed an abrupt junction. The depletion width is then given by (Ref 12:89).

$$W = \frac{2\epsilon_S}{q}\left(\frac{P_{20} + N_{30}}{P_{20}\,N_{30}}\right)(V_B - V) \tag{70}$$

where

ϵ_S = static permittivity (farad/m)

P_{20} = thermal equilibrium hole concentration in region 2

N_{30} = thermal equilibrium electron concentration in region 3

V = voltage across the solar cell, front to back

V_B = built-in voltage of the junction

P_{20} is approximately equal to the concentration of ionized acceptors in region 2. N_{30} is approximately equal to the concentration of ionized donors in region 3.

The built-in voltage is given by (Ref 12:87)

$$V_B = \frac{k_B T}{q} \ln\left(\frac{P_{20}\,N_{30}}{n_{i2}^2}\right) \tag{71}$$

where

k_B = Boltzman's constant (1.38×10^{-23} J/^oK)

T = absolute temperature (^oK)

$n_{i_2} = n_{i_3}$ = the intrinsic carrier density of regions 2 and 3

The current due to electron-hole recombination in the depletion region is assumed to be the dominant dark current. According to the Sah-Noyce-Shockley theory (Ref 10), the diode durrent density has a maximum value of

$$J_D = \frac{q\, n_{i_2}\, W\, D_2 D_3}{L_2 L_3} \cdot \frac{2 \sinh (qV/2k_BT)}{q\,(V_B - V)/k_BT} \cdot \frac{\pi}{2} \qquad (72)$$

This can be approximated by

$$J_D = \frac{q\, n_{i_2}\, W\, D_2 D_3}{2\, L_2 L_3} \left(e^{qV/ak_BT} - 1\right) \qquad (73)$$

where $1 < a < 2$.

The worst **case**, $a = 2$, will be assumed.

The diode current is defined as going from the p side to the n side in the diode or cell, the positive y direction in the cell of Figure 2. However, the photogenerated or short circuit current and the total current are defined as going from the n side to p side within the cell. Therefore, the total current density is given by

$$J^T = J^T_{s.c.} - J_D \qquad (74)$$

If the front and back of the solar cell are connected by a resistanceless wire (short-circuited) then V must be zero. Therefore, $J_D = 0$ and the total current density, J^T, is equal to the photo-generated or short circuit current density $J^T_{s.c.}$.

If the front and back of the solar cell are unconnected (open-circuit) then $J^T = 0$, and

$$J^T_{s.c.} = J_D \tag{75}$$

$J^T_{s.c.}$ is determined by the illumination and is independent of voltage. Eqn (75) determines the open-circuit voltage $V_{o.c.}$, since J_D is a function of voltage.

Under normal operation a load of resistance R is placed across the cell; the cell acts as the source. The condition

$$V = I^T R = J^T AR \tag{76}$$

where A = area of the solar cell

must be satisfied. Eqn (76) determines the voltage, V, and the current density, J^T, of the solar cell since J^T is a function of voltage. As R goes from 0 to ∞ J^T goes from $J_{s.c.}$ to 0 and V goes from 0 to $V_{o.c.}$. A typical current density versus voltage curve for a solar cell is shown in Figure 2.

The power output P_{out} of the cell is given by

$$P_{out} = J^T A\, V \tag{77}$$

The efficiency η is given by

$$\eta = \frac{P_{out}}{P_{in}} = \frac{J^T V}{P_{in}/A} \tag{78}$$

For a given illumination P_{in}/A is a constant. Therefore the maximum η and maximum P_{out} occur when the product of J^T and V is a maximum. This

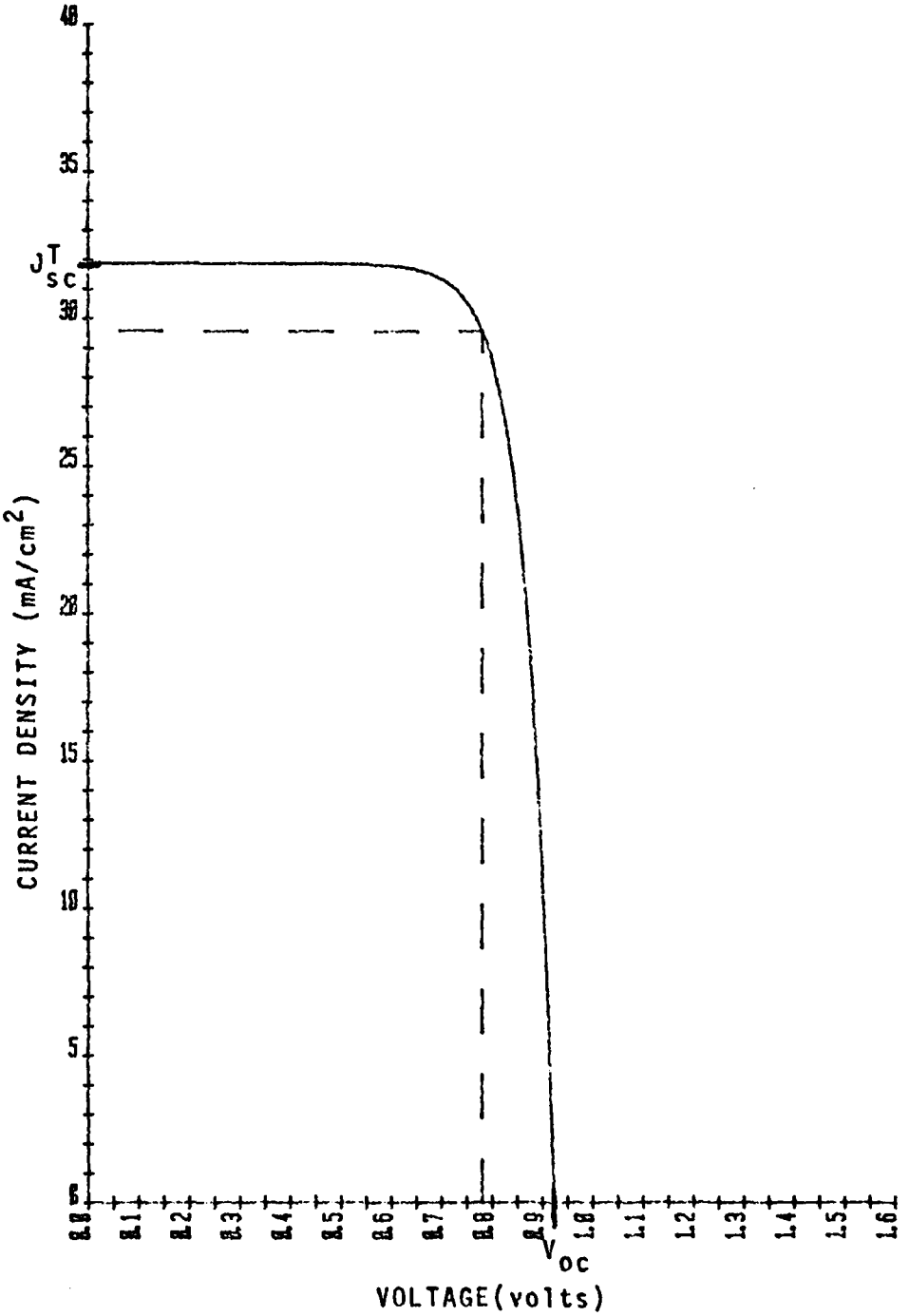

Figure 2. Typical J-V Characteristic of a Solar Cell

optimum operating point is indicated by the dotted lines in Figure 2. η at this point is usually referred to as the efficiency of the solar cell.

Note that decreasing the photogenerated current density $J_{s.c.}^{T}$ shifts the curve in Figure 2 down.

IV Operating Conditions, Design Parameters, and Material Characteristics

The preceding chapters give the gross characteristics of the solar cell, such as $J_{S.C.}^{T}$ and η, in terms of many parameters whose values have not yet been specified. Some of these parameters are operating conditions such as temperature. The conditions under which the model solar cell is assumed to be operating will be specified in this chapter. Some of the parameters are design parameters. It is important to note that some design decisions were already made. They are implied by structure and energy diagram of Figure 1, by the boundary conditions used in Chapter 2, and by other assumptions already made. These require certain limits on the design parameters. These limits are clearly stated in this chapter. Some design parameters are left as variables that can be altered on different computer runs. Other design parameters will be specified in order to reduce the complexity of the computer model.

Many of the material characteristics depend on design parameters. The doping levels and Al contents of the various regions are design parameters because they affect the material's electrical and light absorption properties. The material properties of AlGaAs used in the computer model are specified or given in terms of design parameters. This is the most difficult and least accurate task attempted in this report. The great advantage of ternary compounds like AlGaAs is that they give the designer the choice of a spectrum of materials and material characteristics. However, this poses the problem of determining the characteristics of the material as a function of the added dimension. Modeling of some material properties is also difficult because they are fabrication dependent.

Temperature

The solar cell is assumed to have a temperature, T, of 300°K. Most information on AlGaAs is specified at this temperature. This is also the temperature at which results for solar cells are commonly reported.

Incident Light

The light incident on the cell is specified as sunlight in space near the earth at normal incidence, since the cell is intended for space applications. These conditions are referred to as AMO (Air Mass Zero) conditions. The solar spectral irradiance, $P(\lambda)$, for AMO conditions proposed by Thekaekara, et al (Ref 14:74) is used in this study. $P(\lambda)$ is shown in Figure 3.

The total irradiance or power per unit area was determined by Thekaekara, et al (Ref 14:75) to be

$$\frac{P_{in}}{A} = \int_0^\infty P(\lambda)\, d\lambda = .13530 \text{ watts/cm}^2 \tag{79}$$

This is used in Eqn (78) to determine the efficiency of the solar cell.

The energy of a photon of wavelength λ is

$$E = \frac{hc}{\lambda} \tag{80}$$

where h = Planck's constant (6.626×10^{-34} joule sec)

c = speed of light (2.998×10^{8} m/sec)

The spectral photon flux incident on the solar cell is then

$$F_O(\lambda) = \frac{P(\lambda)}{E} \tag{81}$$

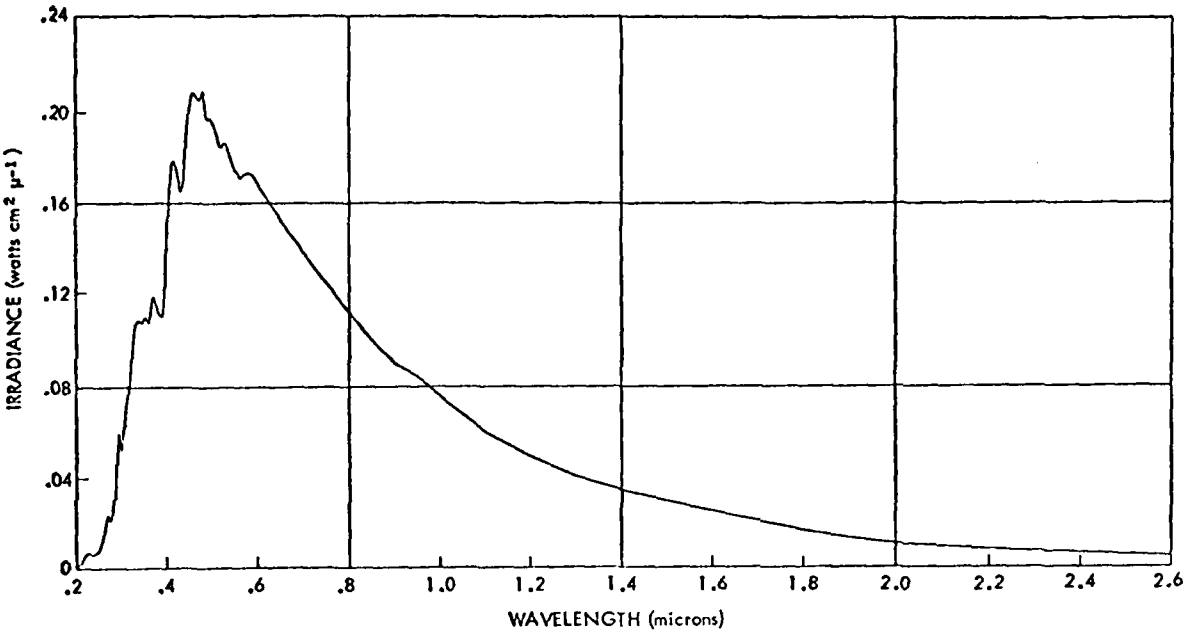

Figure 3. Solar Spectral Irradiance for Air Mass Zero Conditions (Ref 14:74)

Reflectivity

An uncoated GaAs solar cell with an AlGaAs window has a reflectivity, $R(\lambda)$, greater than .30 at all wavelengths of interest (Ref 9). A two-layer anti-reflection coating has reduced $R(\lambda)$ to between .02 and .05 for λ between .4μ and .88μ (Ref 9). In the present study, $R(\lambda)$ is assumed to be .03 for $.35\mu < \lambda > .9\mu$ and 1 at all other wavelengths. This light passed corresponds to photon energies of $1.378\text{eV} < E < 3.542$ eV. If longer wavelength photons were passed into the cell they would produce almost no photogenerated carriers, since their energies are less than the band gap energies of all regions. If higher frequency photons were passed into the cell the effect would also be small, since photon flux for $\lambda < .35\mu$ is small.

The spectral photon flux passed into region 1 is

$$F_1(\lambda) = (1 - R(\lambda))\, F_o\, (\lambda) \tag{82}$$

The spectral photon flux entering each of the other regions is determined by Eqn (31b).

Widths of Regions

The width of each region is a design parameter and is left as a variable in the computer model. However, there are constraints on these variables. Since quantum mechanical tunneling of minority carriers through the barriers (regions 1 and 4) was neglected in the derivation of $J^T_{s.c.}$ in Chapter 2, the width of these barriers must be large enough to make tunneling negligible. In addition, practical limits exist on how thin a layer can be made. The constraints used for the region widths are indicated in Table I.

Table I

Some of the Parameters used in the Computer Model

Parameters (Units)	Region 1	Region 2	Region 3	Region 4
Z (μ)	$Z_1 > 0.3$	$Z_2 > 0.3$	$Z_3 > 0.3$	$Z_4 > 1.0$
X	.9	$X_2 < .25$	$X_3 = X_2$*	.3
E_Γ (eV)	2.779	Eqn (83)	*	1.798
E_x (eV)	2.128	Eqn (84)	*	1.950
E_Γ, (eV)	3.66	Eqn (85)	*	3.06
$\alpha(\lambda)$ (cm^{-1})	Eqn (87)	Eqn (87)	*	Eqn (87)
M_m	.79 +	Eqn (90)+	*	.092
M_p	.65	.65	* +	.65 +
n_i (cm^{-3})	-	Eqn (96)	*	-
K_s	11.1	Eqn (98)	*	12.4
K_d	8.7	Eqn (99)	*	10.1
Dopant	B_e	B_e	T_e	T_e
E_i (eV)	.0424	Eqn (102)	Eqn (101)	.00467
P_o ($10^{17} cm^{-3}$)	7.095	Eqn (117)	-	-
N_o ($10^{17} cm^{-3}$)	-	-	Eqn (115)	4.139
L (μ)	2	2	2	2
μ ($cm^2/V \cdot sec$)	99.4	Eqn (119)	Eqn (121)	164
D (cm^2/sec)	2.57	Eqn (122)	Eqn (122)	4.23

+ = relative mass of minority carrier

* = same value as in region 2

If Z_1 is increased above 0.3μ there is slightly more photogeneration in region 1 and less in the more favorable regions next to the p-n junction, so $J_{S.C.}^{T}$ and η are decreased. Therefore, Z_1 is held at 0.3μ in all computer runs, although it is left as a variable in the program since it is easy to do so. For practical solar cell dimensions little photogeneration will take place in region 4. Z_4 has little affect on cell efficiency as long as it is large enough to prevent significant tunneling of holes from region 3 to region 5. Z_2 and Z_3 are the dimensions of primary interest. Their affect is examined in the next chapter.

Al Content of Regions

As discussed in Chapter 2, the relative Al content of the various regions must be chosen such that the B.C.s used in deriving the photogenerated current are valid. The Al content of regions 1 through 4 are indicated in Table I. The Al content of regions 2 and 3 are the same ($X_2 = X_3$) and are left as a single program variable.

Energy Band Edges

In AlGaAs the maximum in the two highest valence bands occurs where the momentum vector, K, is zero. Two of the three valence bands are degenerate at K = 0 and the split-off band is ignored. Three minima occur in the lowest conduction band. The electron potential energy level at these minima relative to that of the maxima in the valence band are E_Γ, at K = 0, E_X, at the minima along the ⟨100⟩ lattice direction, and E_L, at the minima along the ⟨111⟩ lattice direction. These energies in eV vary with Al content (Ref 8).

$$E_\Gamma = 1.424 + 1.247\ X \text{ eV for } X < .45$$

$$1.424 + 1.247\ X + 1.147\ (X-0.45)^2 \text{eV for } X > .45 \quad (83)$$

$$E_X = 1.900 + 0.125\ X + 0.143\ X^2 \text{ eV} \quad (84)$$

$$E_L = 1.708 + 0.642\ X \text{ eV} \quad (85)$$

Figure 4 shows the dependence of the band edges on Al content.

AlGaAs has a direct-indirect crossover at X = 0.45. For X < .45 the material is a direct semiconductor, since E_Γ is the lowest energy. For X > .45 the material is an indirect semiconductor, since E_X is the lowest energy. For the Al contents of interest the L minimum has little affect and will be ignored because it is an indirect minima and because E_L is always sufficiently higher than one of the other two energy levels, E_Γ and E_X.

The minima at K = 0 in the second lowest conduction may have some affect on absorption (and photogeneration) at small wavelengths. The dependence of the energy of this minima, the Γ' minima, is given by (Ref 6:3142)

$$E_{\Gamma'} = 2.90 + 0.36X + 0.54X^2 \quad (86)$$

The pertinent band energies for each region are indicated in Table I.

Absorption Coefficient

The semiempirical absorption model of Hutcby and Fudurich (Ref 6) is used here. The constants introduced in this section are also taken from their paper.

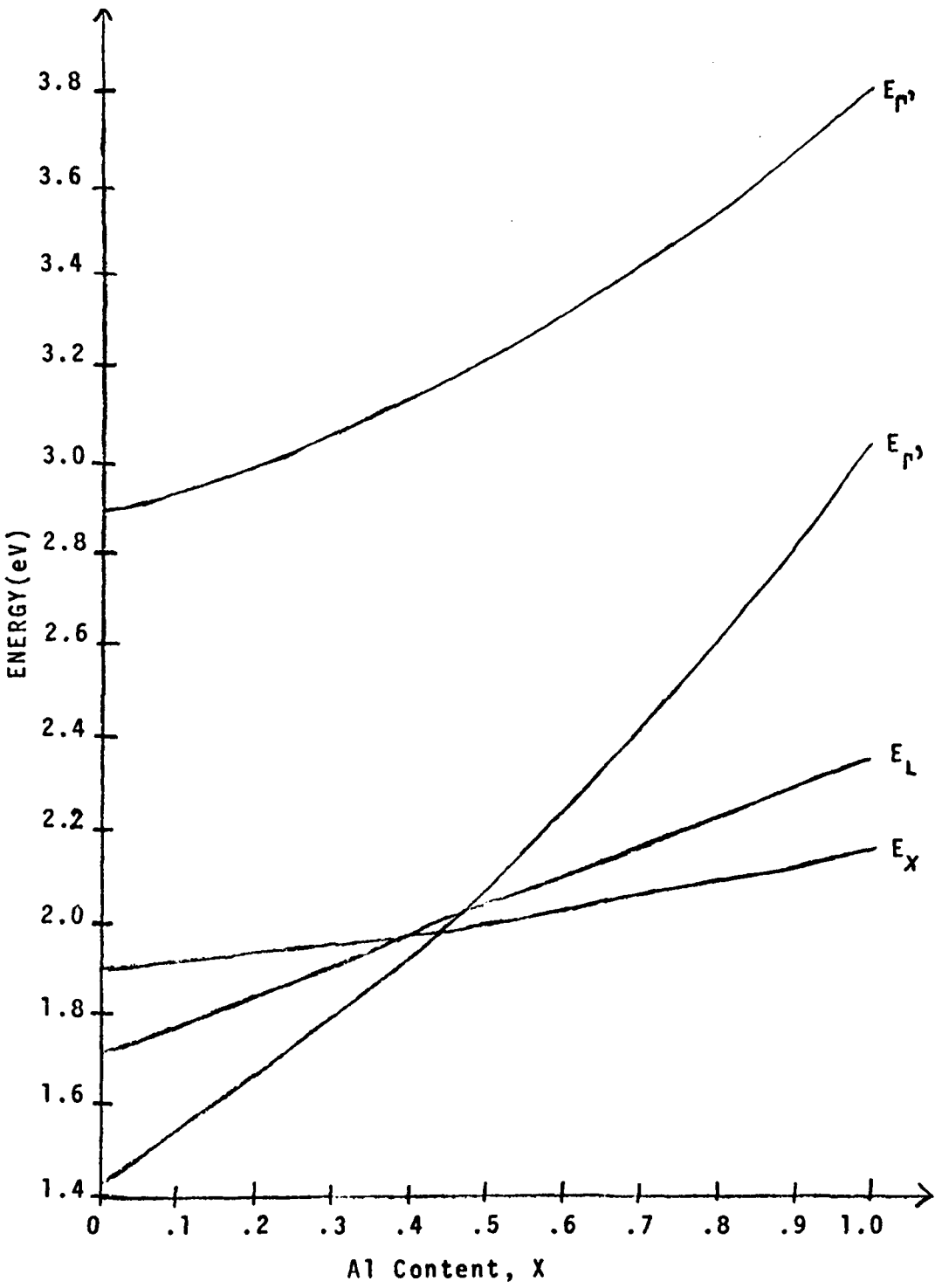

Figure 4. Band Edges as a function of Al Content, X, in $Al_XGa_{1-X}As$ (Ref 8; 6:3142)

The absorption coefficient, α , is a function of the wavelength of light, λ, or its corresponding photon energy, $E = hc/\lambda$. It is also dependent on the shape of the valence and conduction bands, in particular the energies of the minima in the conduction band. Therefore, $\alpha(\lambda)$ is dependent on the Al content and is in general different in each region.

The absorption coefficient is assumed to be the sum of three absorption coefficients (E_Γ, E_X, and E_Γ' respectively).

$$\alpha(\lambda) = \alpha_\Gamma + \alpha_X + \alpha_\Gamma' \tag{87}$$

where

$$\alpha_\Gamma = \begin{cases} A_E \exp\left(\frac{E-E_\Gamma}{E_E}\right) & \text{for } E < E_\Gamma \\ A_\Gamma \cdot (E-E_\Gamma)^{1/2} & \text{for } E > E \end{cases}$$

$$\alpha_X = \begin{cases} 0 & \text{for } E < E_X \\ A_X \cdot (E-E_X)^2 & \text{for } E > E_X \end{cases}$$

$$\alpha_\Gamma' = \begin{cases} 0 & \text{for } E < E_\Gamma' \\ A_\Gamma, \cdot (E-E_\Gamma,)^{1/2} & \text{for } E > E_\Gamma' \end{cases}$$

and where $A_E = 1.9 \times 10^3$ cm^{-1}

$E_E = 1.16 \times 10^{-2}$ eV

$A_\Gamma = 4.0 \times 10^4$ cm^{-1} eV$^{-1/2}$

$A_X = 1.0 \times 10^3$ cm^{-1} eV^{-2}

$A_\Gamma' = 3.5 \times 10^5$ cm^{-1} eV$^{-1/2}$

Relative Carrier Effective Masses

The effective mass of a carrier is a measure of its inertia, or a measure of how much energy is needed to change its momentum. The effective mass of an electron is determined by the curvature of the conduction band edge, $E_C(k)$.

$$m_n^* = \frac{h}{2\pi \frac{\partial^2 E_C}{\partial k^2}} \tag{88}$$

For convenience the relative electron effective mass is defined as

$$M_n = \frac{m_n^*}{m_o} \tag{89}$$

where

m_o = electron rest mass (9.11×10^{-31} kg)

In regions 2, 3, and 4 most of the free electrons are near the Γ minima in the conduction band, since it has the lowest energy. The relative effective mass at the Γ minima varies with Al content according to (Ref 8).

$$M_\Gamma = 0.067 + 0.083X \tag{90}$$

In region 1 most of the free electrons are near the X minima in the conduction band. The relative effective mass at the minima also varies with Al content (Ref 8).

$$M_X = 0.85 - 0.07X \tag{91}$$

Two degenerate valence bands are at their common maximum at $k = 0$, as previously mentioned. The bands have different curvatures, so the holes in each have different effective masses. The relative light-hole

effective mass (M_{lh}), relative heavy-hole effective mass (M_{hh}), and overall relative density of states hole effective mass ($M_p = M_{dh}$) are independent of Al content and are given by (Ref 4:CS-6)

$$M_{lh} = 0.12 \tag{92}$$

$$M_{hh} = 0.62 \tag{93}$$

$$M_p = M_{dh} = (M_{lh}^{3/2} + M_{hh}^{3/2})^{2/3} = 0.65 \tag{94}$$

Intrinsic Carrier Density

The intrinsic carrier densities in regions 2 and 3 are the same, since both regions have the same Al content. The band gap is $E_{\Gamma 2}$ because it is lower than the other band edges. The intrinsic carrier density in regions 2 and 3 is (Ref 12:27)

$$n_{i2} = n_{i3} = 2 \cdot \left(\frac{2 K_B T}{h^2}\right)^{3/2} \cdot (m_{n2}^* m_{p2}^*)^{3/4} \exp(-E_{\Gamma 2}/2 K_B T) \tag{95}$$

which can be simplified to

$$n_{i2} = n_{i3} = 2.51 \times 10^{19} \cdot (M_{n2} M_{p2})^{3/4} \cdot \exp(-E_{\Gamma 2}/0.05170 \text{ eV}) \cdot \text{cm}^{-3} \tag{96}$$

The diode current density, J_D, in Eqn (73) is roughly proportional to n_{i2}. n_{i2} is a strong function of $E_{\Gamma 2}$. As X_2 increases, $E_{\Gamma 2}$ increases, n_{i2} decreases, and J_D decreases.

Static and Dynamic Dielectric Constants

Harrison and Hauser (Ref 5:298) have developed a model for the static dielectric constant, K_S, and dynamic dielectric constant, K_d, for

ternary compounds. Applying their model to AlGaAs,

$$K_{s,d} = \frac{1 + 2\left[X \cdot \frac{K^A_{s,d}-1}{K_{s,d}+2} + (1-X)\frac{K^G_{s,d}-1}{K^G_{s,d}+2}\right]}{1 - X \cdot \frac{K^A_{s,d}-1}{K^A_{s,d}+2} - (1-X)\frac{K^G_{s,d}-1}{K_{s,d}+2}} \tag{97}$$

where

K_s = static dielectric constant of AlGaAs

K_d = dynamic " " " AlGaAs

K^A_s = static " " " AlAs

K^A_d = dynamic " " " AlAs

K^G_s = static " " " GaAs

K^G_d = dynamic " " " GaAs

The following dielectric constants are used for AlAs and GaAs (Ref 11:75):

$$K^A_s = 10.9 \qquad K^A_d = 8.5$$

$$K^G_s = 13.2 \qquad K^G_d = 10.9$$

Using these constants in Eqn (97) gives the dielectric constants for AlGaAs as a function of Al content.

$$K_s = \frac{2.60 - 0.70\ X}{0.197 - 0.035\ X} \tag{98}$$

$$K_d = \frac{2.54 - 0.106\ X}{0.233 - 0.053\ X} \tag{99}$$

Dopants and Ionization Energies

The ionization energy, E_i, of a dopant in a particular semiconductor determines the fraction of dopant atoms ionized. B_e (Beryllium) is used as the p dopant in regions 1 and 2, and T_e (Tellurium) is used as the n dopant in regions 3, 4, and 5. B_e has an ionization energy of 0.030 eV in GaAs (Ref 7). T_e has an ionization energy of 0.003 eV in GaAs (Ref 13). The ionization energy is roughly proportional to the conductivity effective mass (of conduction electrons for donors, and of holes for acceptors) and inversely proportional to the square of the static dielectric constant (Ref 12: 29). The conductivity effective mass and density of states effective mass are approximately equal for III - V semiconductors. The ionization energy of T_e as a donor in AlGaAs is given by

$$E_i = \left(\frac{K_s^G}{K_s}\right)^2 \cdot \frac{M_n}{M_n^G} \cdot E_i^G \qquad (100)$$

where G indicates GaAs. More simply, for regions 3, 4, and 5

$$E_i = \left(\frac{13.2}{K_s}\right)^2 \cdot \frac{M_n}{.067} \cdot (.003 \text{ eV}) \qquad (101)$$

Since the hole effective mass is independent of Al content and even simpler result applies to the ionization energy of B_e as an acceptor in region 1 and 2.

$$E_i = \left(\frac{13.2}{K_s}\right)^2 \cdot (.030 \text{ eV}) \qquad (102)$$

Doping Levels

As already mentioned, the solar cell has been designed to constrain minority carriers to flow toward the junction. However, it is

also desirable to allow majority carriers to flow easily away from the junction. If the potential energy of electrons in region 4 is higher than in region 3, the electrons will not move easily from region 3 to region 4. This problem would show up as an internal resistance. The electron thermal equilibrium concentration in region 4 is required to be greater than or equal to that in region 3.

$$N_{40} > N_{30} \tag{103}$$

Since regions 3 and 4 are in contact some electrons from region 4 will cross the boundary, causing a net negative charge near the boundary in region 3 and a net positive charge in region 4. Consequently, an electric field exists across the boundary, which allows easy flow of electrons from region 3 to region 4.

In order to derive the requirement on the total concentration of donors (ionized and unionized) in regions 3 and 4, the following definitions are made:

N_D^o = total concentration of donor atoms

N_{D3}^t = concentration of ionized donors

N_C - density of states in the conduction band

$$N_C = 2 \left(\frac{2\pi m_n^* k_B T}{h^2}\right)^{3/2}$$

g = degenerary of the conduction band

$g_5 = g_3 = g_4 = 2$ (one for each spin)

E_F = Fermi level

E_C = Conduction band energy

E_D = donor energy level

$E_i = E_C - E_D$ = donor ionization energy

$$N^* = \frac{1}{g} N_C \, e^{-E_i/k_BT}$$

The concentration of unionized donors is given by the Fermi-Dirac distribution.

$$N_D^o - N_D^t = \frac{N_D^o}{1 + \frac{1}{g} e^{(E_D - E_F)/k_BT}} \tag{104}$$

So,

$$N_D^t = N_D^o \left[1 - \frac{1}{\frac{1+e^{(E_C-E_F)/k_BT}}{N_C} \cdot \frac{N_C e^{(E_D-E_C)/k_BT}}{g}} \right] \tag{105}$$

But,

$$N_o = N_C \, e^{-(E_{C4}-E_F)/k_BT} \tag{106}$$

Therefore,

$$N_D^t = N_D^o \left(1 - \frac{1}{1 + N^*/N_o} \right) \tag{107}$$

$$N_D^t = \frac{N_D^o \, N^*}{N_o + N^*} \tag{108}$$

The thermal equilibrium concentration can also be written as

$$N_o = P_o + N_D^t = \frac{n_i^2}{N_o} + N_D^t \tag{109}$$

$$N_o = \frac{n_i^2}{N_o} + \frac{N_D^o \, N^*}{N_o + N^*} \tag{110}$$

$$N_o = \frac{n_i^2 \, (N_o + N^*) + N_D^o \, N^* \, N_o}{N_o (N_o + N^*)} \tag{111}$$

$$N_o^2 = (N_o + N^*) = n_i^2 \, (N_o + N^*) + N_D^o \, N_4^* \, N_o \tag{112}$$

$$(N_o^2 - n_i^2) \, (N_o + N^*) = N_D^o \, N^* \, N_o \tag{113}$$

For high doping levels $N_o^2 >> n_i^2$ so

$$N_o^2 \ (N_o + N^*) \cong N_D^o \ N^* \ N_o \tag{114}$$

Solving for N_o

$$N_o = \frac{N^*}{2}\left[\sqrt{1 + \frac{4N_D^o}{N^*}} - 1\right] \tag{115}$$

Eqn (115) applies to regions 3, 4, and 5. $N_{D_4}^o$ is chosen to be 1×10^{18} cm^{-3}, which implies $N_{40} = 4.139 \times 10^{17}$ cm^{-3}. Eqn (103) is easily satisfied for $N_{D_3}^o < 1 \times 10^{18}$ cm^{-3} and $X_3 < .3$ as demonstrated in the following Table for $N_{D_3}^o = 1 \times 10^{18}$ cm^{-3}

X	N_{30} (cm^{-3})
0	3.538×10^{17}
.1	3.758×10^{17}
.2	3.959×10^{17}
.3	4.139×10^{17}

A requirement similar to Eqn (103) applies regions 4 and 5.

$$N_{50} > N_{40} \tag{116}$$

$N_{D_5}^o$ is chosen to be 1.5×10^{18} cm^{-3}, which implies $N_{50} = 4.508 \times 10^{17}$cm^{-3}, so that this condition is satisfied.

The thermal equilibrium hole concentrations in regions 1 and 2 are determined by an equation similar to Eqn (115).

$$P_o = \frac{p^*}{2}\left[\sqrt{1 + \frac{4N_A^o}{p^*}} - 1\right] \tag{117}$$

where

N_A^o = total concentration of acceptor atoms

$$p^* = \frac{N_v}{g} e^{-Ei/k_BT}$$

g = 4 (two degenerate bands x 2 spins)

$$N_n = 2 \left(\frac{2 m_p^* k_B T}{h^2}\right)^{3/2} = \text{density of states in the valence band}$$

The doping requirement for regions 1 and 2 is

$$P_{20} > P_{10} \tag{118}$$

N_{A1}^o is chosen to be 1.5×10^{18} cm^{-3}, which implies $P_{10} = 7.095 \times 10^{17}$ cm^{-3}. Eqn (118) is then easily satisfied for $N_{A2}^o < 1 \times 10^{18}$ cm^{-3}. In all computer runs P_{20} and N_{30} were printed out to insure that Eqns (103) and (118) were satisfied.

Minority Mobilities and Diffusivities

The model of Sutherland and Hauser (Ref 11:62-64, 76) is used in this section to determine the minority carriers mobilities. The model is based on the assumption that mobility is primarily determined by a polar optical phonon scattering process.

In region 2, virtually all conduction electrons are in the direct valley (Γ). This is also true of GaAs. The electron mobility in region 2 is then related to the electron mobility in GaAs (G indicates GaAs).

$$\mu_2 = \left(\frac{M^G}{M}\right)^{3/2} \left[\frac{\frac{1}{K_d^G} - \frac{1}{K_s^G}}{\frac{1}{K_d} - \frac{1}{K_s}}\right] \mu_n^G (P_{20}) \tag{119}$$

where the mobility in GaAs, μ_n^G, is determined by the concentration of ions (P_{20})

$$\mu_n^G (P_{20}) = \frac{720 \text{ cm}^2/\text{ V} \cdot \text{sec}}{1 + (5.51 \times 10^{-17} \text{ cm}^3) P_{20}^{(.233)}}$$

In region 1 virtually all conduction electrons are near the X minima, just as in AlAs. The mobility of electrons in region 1 is then related to the mobility in AlAs (A indicates AlAs).

$$\mu_1 = \left(\frac{M^A}{M}\right)^{3/2} \cdot \left[\frac{\frac{1}{K_d^A} - \frac{1}{K_s^A}}{\frac{1}{K_d} - \frac{1}{K_s}}\right] \cdot \mu_n^A (P_{10}) \qquad (120)$$

where

$$\mu_n^A (P_{10}) = \frac{165 \text{ cm}^2/\text{V} \cdot \text{sec}}{1 + (8.1 \times 10^{-17} \text{ cm}^3)\ P_{10}^{(.13)}}$$

In regions 3 and 4 the hole mobilities are given by

$$\mu_{3,4} = \left[\frac{\frac{1}{K_d^G} - \frac{1}{K_s^G}}{\frac{1}{K_d} - \frac{1}{K_s}}\right] \cdot \mu_p^G (N_o) \qquad (121)$$

where $$\mu_p^G(N_o) = \frac{380 \text{ cm}^2/\text{V} \cdot \text{sec}}{1 + (3.17 \times 10^{-17} \text{cm}^3) N_o^{(.266)}}$$

The diffusivities in each region are determined by the Einstein relation.

$$D = \frac{k_B T}{q} \mu \qquad (122)$$

Diffusion Lengths

Diffusion lengths are very fabrication dependent. Even when using the same technique and same equipment experimenters obtain samples with widely varying diffusion lengths. For this reason a conservative value of 2μ will be used in all regions.

Surface Recombination Velocities

Surface recombination velocities are also fabrication dependent. Therefore, they are left as variables in the program. A typical value is 10^4 cm/sec. For convenience all three surface recombination velocities will be varied together ($S = S_o = S_1 = S_3$).

V. Computer Model and Results

A description of the program used to model the AlGaAs solar cell is described in this chapter. The results of varying some of the parameters are presented and discussed. It should be noted that this chapter does not include the entire results of this report. In particular, the theoretical results discussed in Chapter II are fairly general and include important statements on multi-layered solar cells.

Description of Program

The program used to model the cell is based on the results of the previous three chapters. The inputs to the program are X ($= X_2 = X_3$), Z_2, Z_3, and S. Other parameters were left as variables in the program that can easily be changed or made inputs to the program. However, in the present study the four parameters mentioned above are of primary interest. The other variables were held at the following values

$$Z_1 = .3\mu$$

$$Z_4 = 1.0\mu$$

$$N^o_{A2} = 1 \times 10^{18}\ cm^{-3}$$

$$N^o_{D3} = 1 \times 10^{18}\ cm^{-3}$$

$$L_1 = L_2 = L_3 = L_4 = 2\mu$$

The program used the inputs, the above variables, values for parameters specified in Chapter IV, and the Eqns in Chapter IV to calculate all

the parameters needed in Chapters II and III. Table I in Chapter IV indicates many of the parameters specified or given in terms of other parameters. These were then used in Eqns (61) through (64) in Chapter II to compute the spectral current densities. The integration indicated in Eqn (66) was done numerically using wavelength increments of $\Delta\lambda = .01\mu$. $J^T_{s.c.}$ was obtained as in Eqn (67). J_D was determined using Eqns (70) through (73). Eqn (74) was used to determine J^T as a function of V, with increments of $V = .001$ volts. At each V the efficiency, η, was calculated from Eqn (78). These were compared and the maximum η, the efficiency of the cell, found--along with its corresponding J^T - V pair. The open circuit voltage V_{OC} was obtained by interpolating between the points at which J^T was just above and just below zero.

Results

At $S = 10^4$ cm/sec (typical value) the Al content in regions 2 and 3 ($X = X_2 = X_3$) was varied. At X = 0, .05, .01, and .02, Z_2 and Z_3 were varied and the optimum (for maximum efficiency) combination of Z_2 and Z_3 found. At each of these Al contents the optimum values of Z_2 and Z_3 were found to be $Z_2 = 0.50\mu \pm .01\mu$ and $Z_3 = 2.4\mu \pm .1\mu$.

X was then varied in small increments from 0 to .25 and some of the characteristic of the cell noted. These characteristics are presented in Table II. The efficiency, η, was found to be relatively independent of X for $0 < X < .15$. The optimum value of X was X = .05 where $\eta = 17.71\%$. However, this is only .23% higher than for X = 0 (plain GaAs) where $\eta = 17.58\%$. η varied in a complicated manner with X over the range $0 < X < .12$ achieving several maxima. η decreased with increasing X for $X > .12$.

Table II

Solar Cell Characteristics for Different Al Content in Regions 2 and 3 ($X = X_2 = X_3$) at $S = 10^4$cm/sec, and Optimum Z_2 and Z_3 ($Z_2 = 0.50\mu$, $Z_3 = 2.4\mu$)

X	J_2^T (mA/cm^2)	J_3^T (mA/cm^2)	$J_{s.c.}^T$ (mA/cm^2)	n_{i2} (cm^{-3})	$V_{o.c.}$ (Volts)	J_n^T (mA/cm^2)	V_n (Volts)	η (%)
0	25.387	7.384	32.771	2.61×10^6	.9275	30.62	.777	17.58
.01	25.040	7.333	32.373	2.07×10^6	.9381	30.30	.788	17.65
.02	24.679	7.244	31.922	1.64×10^6	.9503	29.89	.800	17.67
.03	24.316	7.149	31.465	1.30×10^6	.9746	29.06	.823	17.68
.04	23.947	7.039	30.986	1.03×10^6	.9808	28.92	.811	17.68
.045	23.783	7.014	30.798	9.18×10^5	.9869	28.72	.828	17.70
.05	23.609	6.974	30.583	8.17×10^5	.9869	28.72	.834	17.71
.055	23.411	6.887	30.247	7.28×10^5	.9929	28.45	.840	17.67
.06	23.258	6.881	30.140	6.48×10^5	.9991	28.31	.846	17.70
.07	22.884	6.738	29.622	5.13×10^5	1.0111	27.86	.857	17.65
.08	22.571	6.710	29.281	4.07×10^5	1.0234	27.55	.869	17.69
.09	22.232	6.618	28.850	3.22×10^5	1.0356	27.18	.880	17.68
.10	21.872	6.490	28.362	2.56×10^5	1.0476	26.75	.891	17.62
.11	21.565	6.455	28.019	2.02×10^5	1.0599	26.44	.903	17.64
.12	21.227	6.369	27.596	1.60×10^5	1.0720	26.04	.915	17.61
.13	20.883	6.292	27.175	1.27×10^5	1.0841	25.67	.926	17.57
.14	20.572	6.218	26.790	1.05×10^5	1.0963	25.31	.938	17.55
.15	20.250	6.128	26.378	7.96×10^4	1.1084	24.96	.949	17.50
.16	19.943	6.055	25.998	6.30×10^4	1.1205	24.60	.961	17.47
.18	19.322	5.886	25.208	3.95×10^4	1.1447	23.91	.983	17.37
.20	18.707	5.702	24.410	2.48×10^4	1.1687	23.17	1.006	17.23
.25	17.269	5.363	22.632	7.69×10^3	1.2292	21.54	1.064	16.94

The short circuit current, $J^T_{s.c.}$, decreased steadily with increasing X, while the open circuit voltage, $V_{o.c.}$, increased steadily with increasing X. This is as anticipated. The band gap increases with X and leads to smaller absorption coefficients (especially at large λ), and a smaller intrinsic carrier density n_i (see Table II). The smaller absorption coefficients lead to less photogeneration particularly at large λ. This is evident by comparing Figures 5, 7, and 9, where the spectral current densities for X = 0, .05, and .25 are presented. The J^T versus V plots for these values of X are given in Figures 6, 8, and 10.

The Al content in regions 2 and 3 was also varied at S = 0 and S = 10^7 cm/sec. For S = 0 (no surface recombination) the optimum values of Z_2 and Z_3 were found to be $Z_2 = 0.48\mu$ and $Z_3 = 1.8\mu$ independent of Al content. The results for S = 0 are given in Table III. They are similar to those for S = 10^4. Again the efficiency varied in a complicated manner with X, achieving several local maxima in the range $0 < X < .12$ but decreasing for $X > .12$. The best efficiency, 18.01%, is again just slightly higher than at X = 0 (17.87%). Efficiencies were slightly higher for S = 0 than for S = 10^4 cm/sec because more of the photogenerated minority carriers reach the junction.

The results for S = 10^7 cm/sec are given in Table IV. The efficiency was found to increase steadily with decreasing Z_2 and increasing Z_3 for all X used. A small Z_2 and large Z_3 are otpimum for very large S, because most of the photogenerated minority carriers will then be produced in region 3 near the junction, where the only surface recombination that can affect them is far away at y_3.

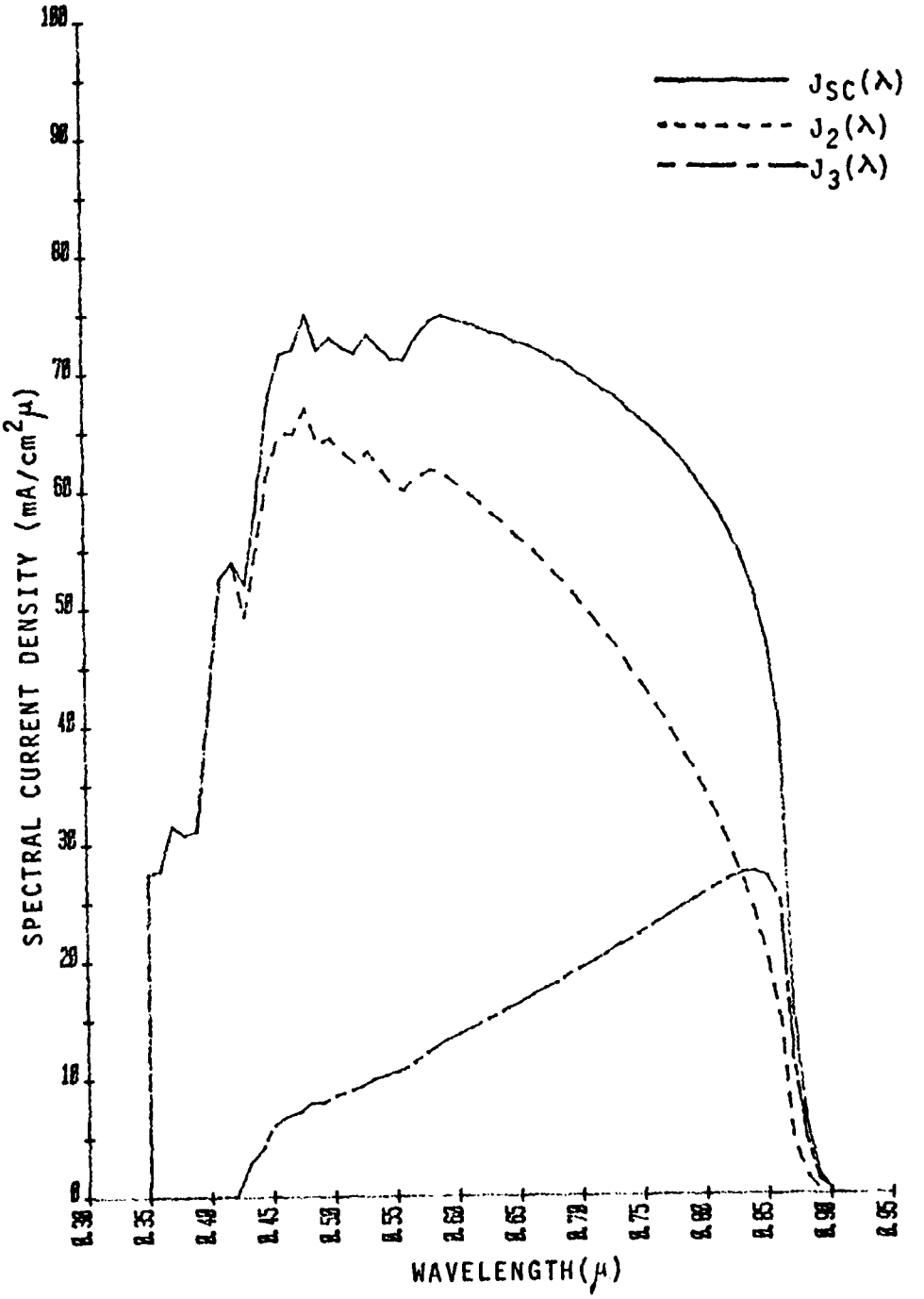

Figure 5. Photogenerated Spectral Current Densities for $S=10^4$ cm/sec, $X=0$, $z_2=0.50\mu$, $z_3=2.4\mu$ (optimum values z_2 and z_3)

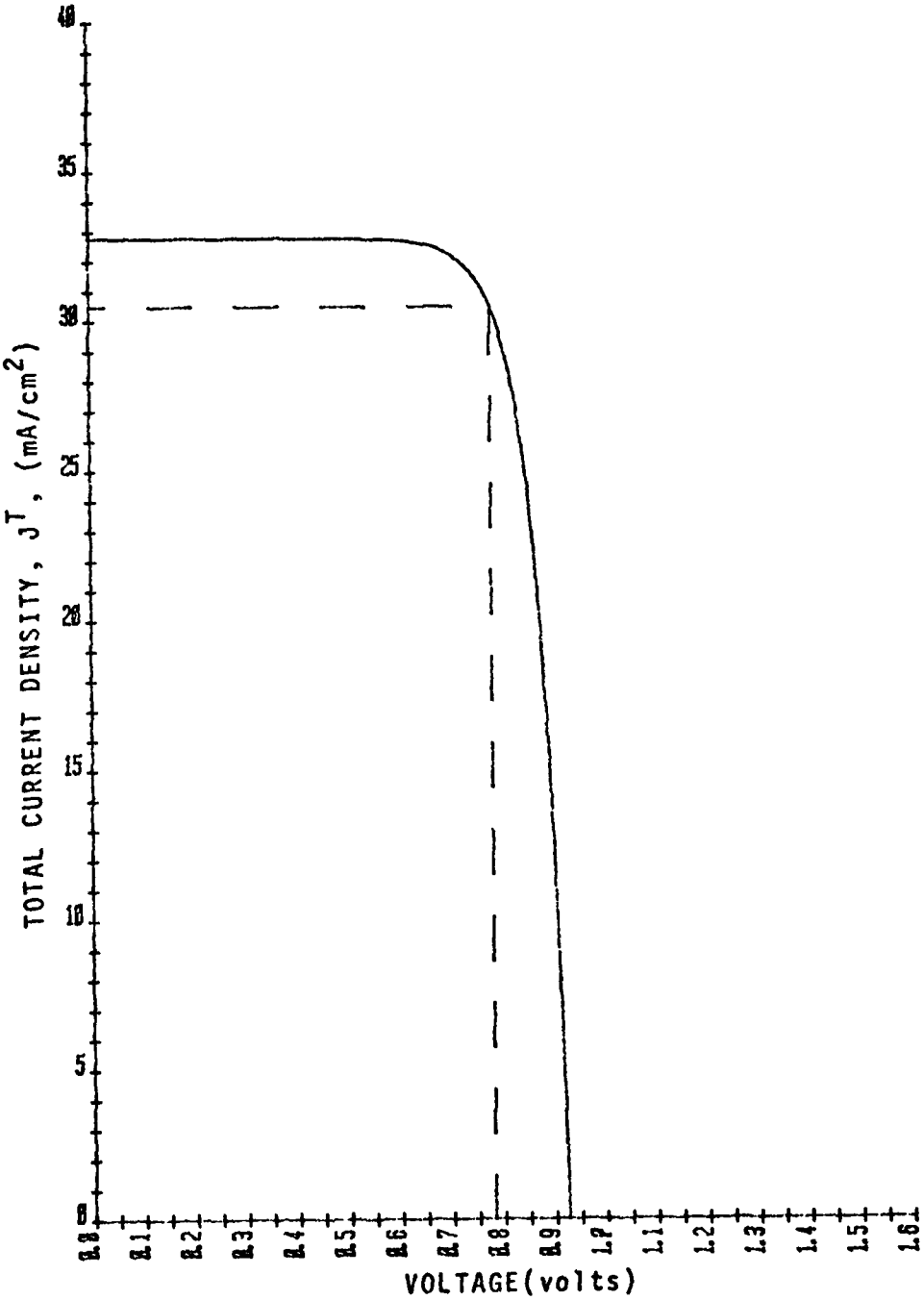

Figure 6. J^T versus V for $S=10^4$cm/sec, $X=0, z_2=0.50\mu$, $z_3=2.4\mu$ (optimum values of z_2 and z_3)

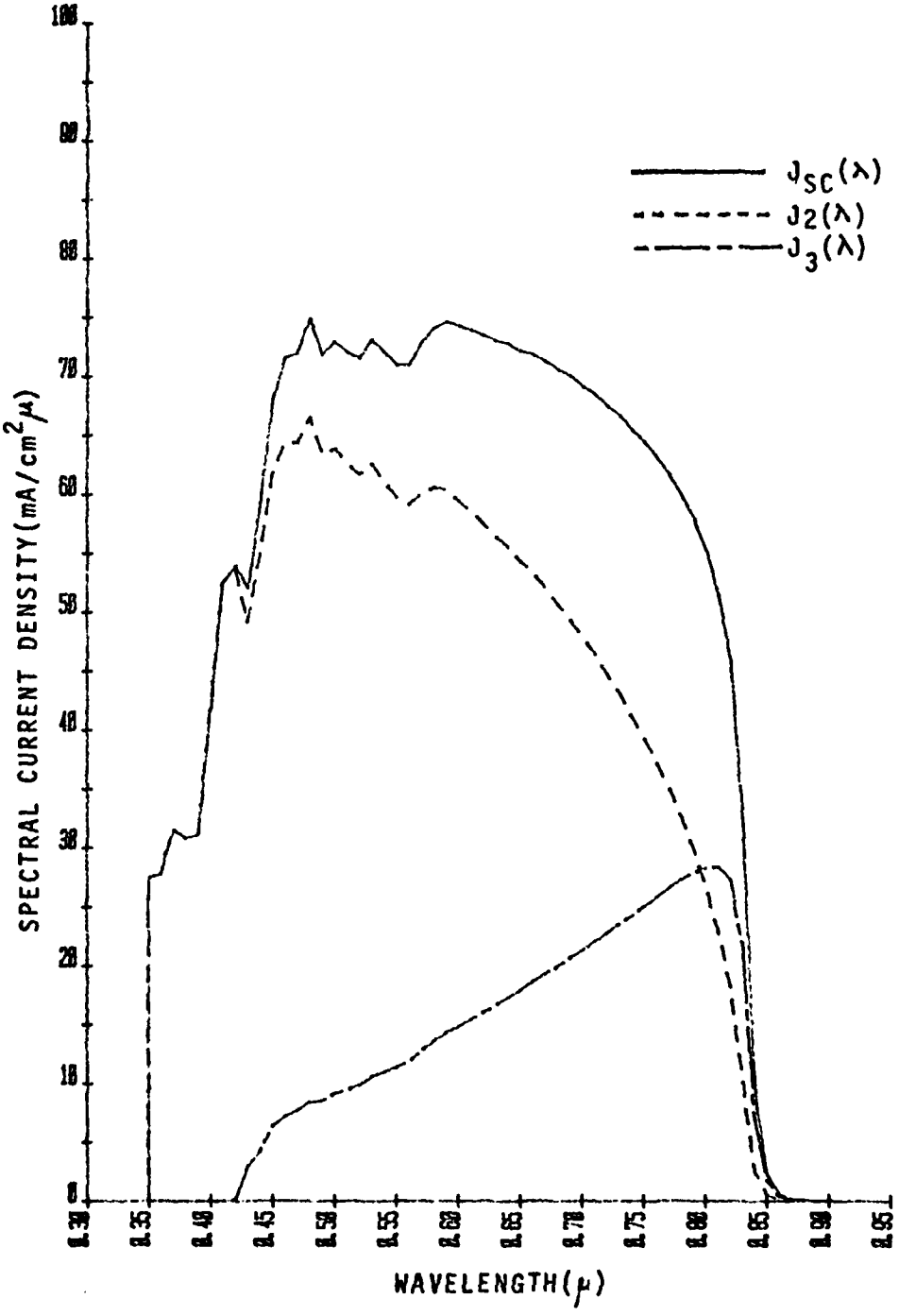

Figure 7. Photogenerated Spectral Current Densities for $S=10^4$cm/sec, X=.05, $z_2=0.50\mu$, $z_3=2.4\mu$ (optimum values of z_2 and z_3)

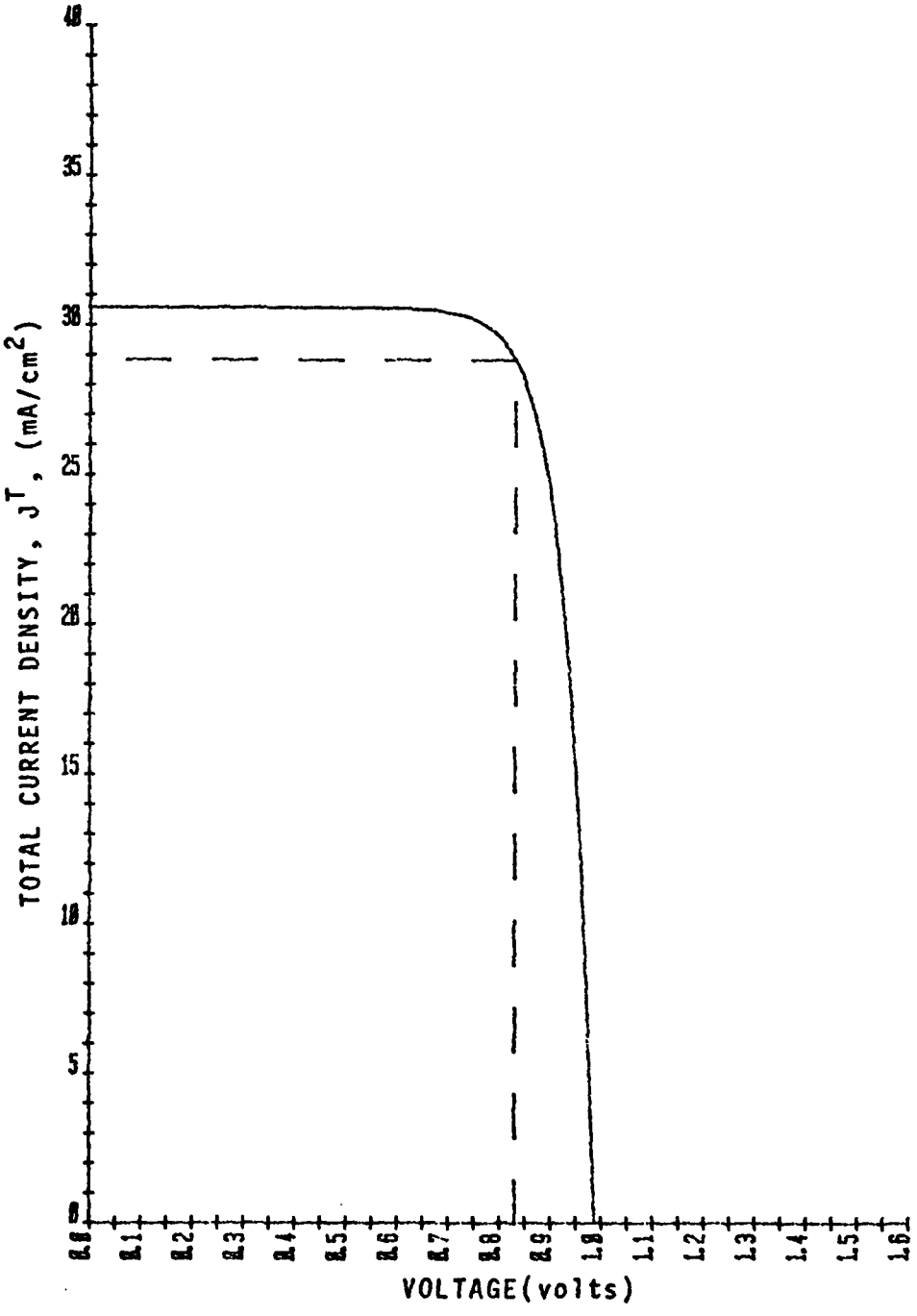

Figure 8. J^T versus V for $S=10^4$cm/sec, X=.05, $z_2=0.50\mu$, $z_3=2.4\mu$ (optimum z_2 and z_3)

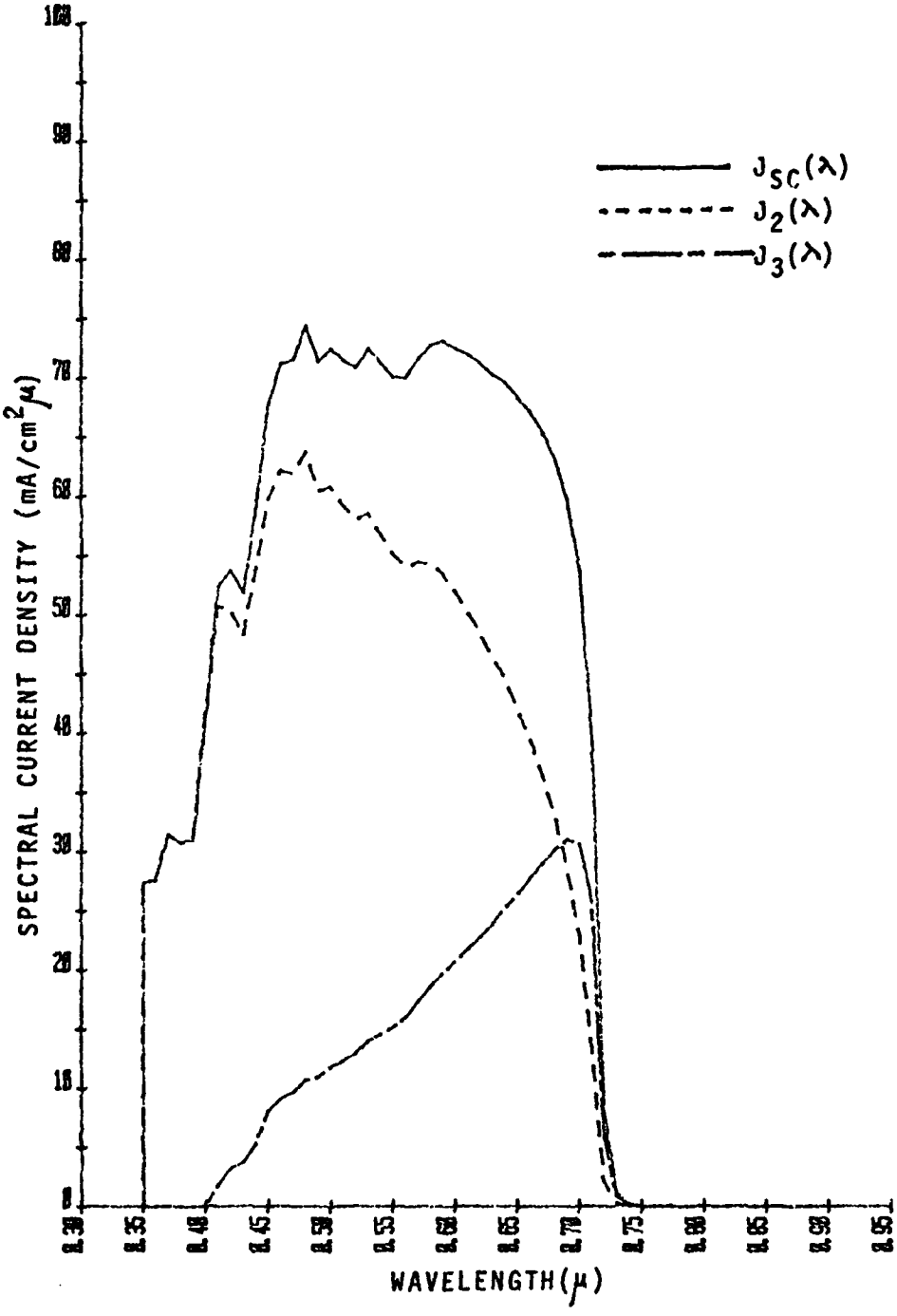

Figure 9. Photogenerated Spectral Current Densities for $S=10^4$cm/sec, $X=.25$, $z_2=0.50\mu$, $z_3=2.4\mu$ (optimum z_2 and z_3)

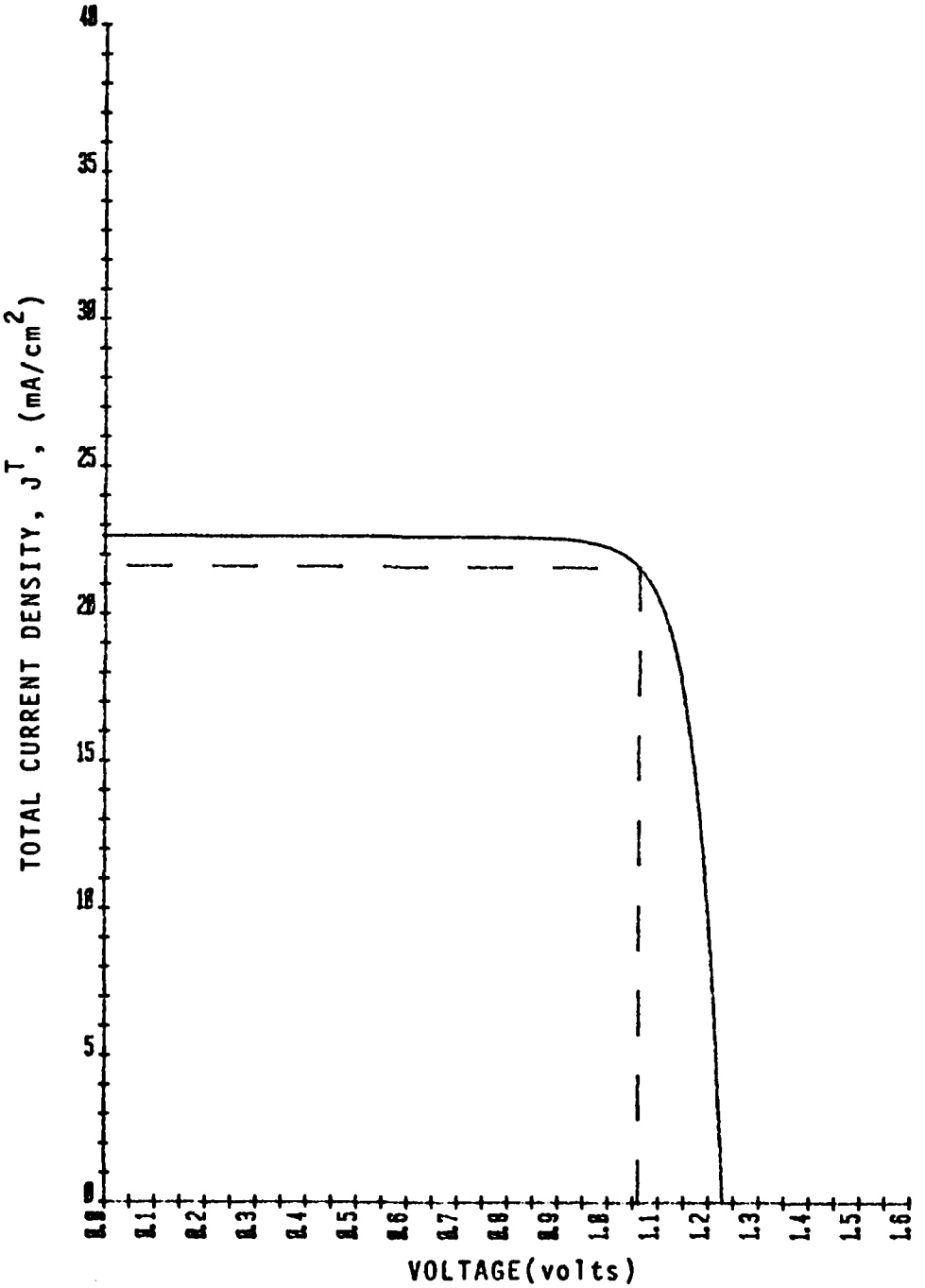

Figure 10. J^T versus V for $S=10^4$cm/sec, X=.25, $z_2=0.50\mu$, $z_3=2.4\mu$ (optimum z_2 and z_3)

Table III

Solar Cell Characteristics for Different Al Content in Regions 2 and 3 ($X = X_2 = X_3$) at $S = 0$, and Optimum Z_2 and Z_3 (Z_2=0.48μ, Z_3=1.8μ)

X	$J^T_{s.c.}$ (mA/cm^2)	$V_{o.c.}$ (Volts)	η (%)
0	33.265	.9266	17.87
.01	32.865	.9389	17.93
.02	32.415	.9511	17.96
.03	31.956	.9633	17.98
.04	31.476	.9755	17.97
.05	31.073	.9878	18.01
.06	30.629	1.0000	18.01
.07	30.110	1.0120	17.96
.08	29.768	1.0243	18.01
.09	29.337	1.0365	18.00
.10	28.848	1.0485	17.94
.11	28.504	1.0608	17.97
.12	28.080	1.0730	17.94
.13	27.658	1.0851	17.90
.14	27.274	1.0973	17.89
.16	26.481	1.1215	17.82
.18	25.691	1.1457	17.72
.22	24.048	1.1938	17.40
.25	23.127	1.2304	17.33

Table IV

Efficiency as a Function of Al Content in Regions 2 and 3 ($X=X_2=X_3$) at $S=10^7$cm/sec, and $Z_2=0.20\mu$ and $Z_3=10\mu$

X	η (%)
0	12.69
.01	12.71
.02	12.70
.03	12.68
.04	12.65
.05	12.65
.06	12.66
.07	12.55
.08	12.57
.09	12.53
.10	12.46
.12	12.42
.15	12.28
.20	11.98
.25	11.69

η increased only slightly (.01%) for Z_3 above 10μ so this value was chosen for comparison. Since it is difficult to make layers smaller than .2μ this value was used for Z_2. The efficiencies were much less than for S = 0 or S = 10^4 cm/sec. Again little was gained by increasing Al content. In fact, for X > .03 η was less than for X = 0. The optimum value of X = .01 gave only a .02% increase in η above that for X = 0 (12.71% versus 12.69%).

VI. Summary and Conclusions

The multi-layered cell indicated in Figure 1 (a solar cell with a window, a single homojunction, and a back-barrier on a base) has been analyzed theoretically under fairly general conditions. The theoretical results are applicable to similarly structured cells made from other materials. The carrier transport equations were solved to obtain the excess minority carrier densities and the short-circuit current density. The back-barrier was proven theoretically to increase the short circuit current and therefore the efficiency of the solar cell. The back-barrier is most useful when low surface recombination velocities can be obtained, and when a large portion of the photogeneration takes place in the region in front of it. The program already developed could be easily modified to model a cell without a back-barrier. The increase in efficiency due to the back-barrier could then be obtained for various conditions.

The properties of $Al_xGa_{1-x}As$ have not been as thoroughly investigated as those of other materials. This problem is compounded because data on these properties is needed as a function of Al content. In this report many of the properties of $Al_xGa_{1-x}As$ have been modeled by drawing on the work of others. Although much research on AlGaAs is still needed, Chapter IV includes a significant up-to-date compilation of information on and models of the properties of this material.

The AlGaAs solar cell was modeled on a computer and some of the design parameters varied in order to examine their effects. The optimum widths of regions 2 and 3 were found to be virtually independent of Al content, X, for $0 < X < .23$, but dependent on the surface recombination velocity.

Only small gains in efficiency (less than 0.3%) were obtained by varying the Al content in regions 2 and 3. However, these results were based on the assumption that the diffusion lengths were independent of Al content. AlGaAs can be expected to have a higher diffusion length than GaAs when made from liquid phase epitaxial growth, since the Al in the melt acts as a gatherer of impurities. This increase in diffusion length would result in a slightly higher short circuit current and a significant improvement in voltage performance and fill-factor (see Eqn (73)). Also the cell analyzed can be used in a concentrator application wherein the voltage operating point would be such that the thermal diffusion dominates the dark current-voltage characteristic resulting in a significant increase in fill-factor.

Since Air Force missions in space are limited to earth orbit, modifications of this cell's design will be required to optimize its performance in radiation belts (electrons and protons) for flat panel applications. However, very little data exists on radiation damage effects to AlGaAs material.

Bibliography

1. Angrist, Stanley W. Direct Energy Conversion (Second Edition). Boston: Allyn and Bacon, Inc., 1971.

2. Bedair, S. M., et al. "Processing-Induced Defects in n-Type $Al_{0.3}Ga_{0.7}As$ LPE Layers." Paper presented at the 11th International Conference on Defects and Radiation in Semiconductors (1980).

3. Bucher, E. "Solar Cell Materials and Their Basic Parameters." Applied Physics, 17: 1-25 (1978).

4. Gibart, Pierre et al. "Cascade Solar Cell" SERI-PR-611-737 Solar Energy Research Institute, Photovoltaic Research Branch Semiannual Report (July 1980).

5. Harrison, J. W. and J. R. Hauser. "Theoretical Calculations of Electron Mobility in Ternary III - V Compounds," Journal of Applied Physics, 47 (1): 292 (January 1976).

6. Hutchby, J. A. and R. L. Fudurich. "Theoretical Analysis of $Al_xGa_{1-x}As$ - GaAs Graded Band-gap Solar Cell," Journal of Applied Physics, 47 (7): 3140 (July 1976).

7. Kressel, H. and F. Z. Hawrylo. "Ionization Energy of Mg and Be Acceptors in GaAs," Journal of Applied Physics, 41: 1865 (1970).

8. Lifshitz, N. et al. "Pressure and Compositional Dependences of the Hall Coefficient in $Al_xGa_{1-x}As$ and Their Significance," Physical Review B, 21 (2):670 (January 1980).

9. Rahilly, W. P. Energy Conversion Branch, Aerospace Power Division, Aero Propulsion Laboratory, Wright-Patterson AFB, Ohio (personal correspondence). 1981.

10. Suh, C. T., R. N. Noyce, and W. Shockley, "Carrier Generation and Recombination in P-N Junctions and P-N Junction Characteristics." Proc. IRE, 45: 1228 (1957).

11. Sutherland, J. E. and J. R. Hauser. "A Theoretical Study of Heterojunction and Gaded Band Gap Type Solar Cells," Annual Report on NASA Grant No. NSG 1116, April 1977.

12. Sze, S. M. Physics of Semiconductor Devices, New York: John Wiley and Sons, 1969.

13. Sze, S. M. and J. C. Irvin, "Resistivity, Mobility and Impurity Levels in GaAs, Ge, and Si at 300°K," Solid State Electron., 11: 599 (1968).

14. Thekaekara, M. P. et al. "The Solar Constant and the Solar Spectrum Measured from a Research Aircraft," NASA TR R-351, National Aeronautics and Space Administration, Washington, DC, October 1970.

15. Wolff, George, et al. "High Efficiency Solar Panel, Phase II, Gallium Arsenide," AFWAL-TR-80-2128, Aero Propulsion Laboratory, AFWAL, Wright-Patterson AFB, Ohio, March 1981.

Vita

David J. Miazza was born on 8 April 1958 in Glen Cove, New York. He received his Bachelor of Science degree in Electrical Engineering in May 1980. Upon graduation, he received a commission in the USAF through the ROTC program. He entered the Electro-Optics Program in the Engineering School at the Air Force Institute of Technology in June 1980.

This thesis was typed by Mrs Anna L. Lloyd.

UNCLASSIFIED

SECURITY CLASSIFICATION OF THIS PAGE (When Data Entered)

REPORT DOCUMENTATION PAGE		READ INSTRUCTIONS BEFORE COMPLETING FORM
1. REPORT NUMBER AFIT/GEO/PH/81D-4	2. GOVT ACCESSION NO. AD-A111 174	3. RECIPIENT'S CATALOG NUMBER
4. TITLE (and Subtitle) THEORETICAL ANALYSIS OF AN AlGaAs/AlGaAs HETEROFACE BACK-BARRIER SOLAR CELL		5. TYPE OF REPORT & PERIOD COVERED MS Thesis 6. PERFORMING ORG. REPORT NUMBER
7. AUTHOR(s) David J. Miazza Second Lieutenant		8. CONTRACT OR GRANT NUMBER(s)
9. PERFORMING ORGANIZATION NAME AND ADDRESS Air Force Institute of Technology (AFIT/ENA) Wright-Patterson AFB, OH 45433		10. PROGRAM ELEMENT, PROJECT, TASK AREA & WORK UNIT NUMBERS
11. CONTROLLING OFFICE NAME AND ADDRESS		12. REPORT DATE December 1981 13. NUMBER OF PAGES 63
14. MONITORING AGENCY NAME & ADDRESS(if different from Controlling Office)		15. SECURITY CLASS. (of this report) Unclassified 15a. DECLASSIFICATION/DOWNGRADING SCHEDULE

16. DISTRIBUTION STATEMENT (of this Report)

Approved for public release; distribution unlimited.

17. DISTRIBUTION STATEMENT (of the abstract entered in Block 20, if different from Report)

28 JAN 1982

18. SUPPLEMENTARY NOTES

Fredric C. Lynch
Major, USAF
Director of Public Affairs

19. KEY WORDS (Continue on reverse side if necessary and identify by block number)

Solar Cell, Aluminum Gallium Arsenide, Gallium Arsenide, p-n junction Heteroface solar cell, Back-Barrier Solar Cell

20. ABSTRACT (Continue on reverse side if necessary and identify by block number)

A solar cell with a high band gap window, a homojunction, and a back-barrier on a base has been analyzed theoretically under fairly general conditions. The carrier transport equations were solved to obtain the short circuit current density. The theoretical results are applicable to similarly structured cells made from other materials. Although there is a lack of data on the properties of AlGaAs, many of the properties of AlGaAs have been modeled in this report by drawing on the work of others. The AlGaAs solar cell was modeled on a computer and certain design parameters (such as Al content) varied in order to examine their effects.

DD FORM 1 JAN 73 1473 EDITION OF 1 NOV 65 IS OBSOLETE

UNCLASSIFIED

SECURITY CLASSIFICATION OF THIS PAGE (When Data Entered)